

63-3-4

404 260

CATALOG  
AS AD 100 404260

DDC  
REPRODUCTION  
MAY 22 1963  
TSM B

FREE-MOLECULE FLOW IN THE AXIAL-FLOW TURBO-VACUUM PUMP

by

John S. Maulbetsch  
Research Assistant

and

Ascher H. Shapiro  
Ford Professor of Engineering

Final Report, March 1963

Office of Naval Research Contract Nonr-1841(55)  
M.I.T. Division of Sponsored Research  
Project No. DSR 7-8120

FLUID MECHANICS LABORATORY

Department of Mechanical Engineering  
Massachusetts Institute of Technology  
Cambridge, Massachusetts

Table of Contents

	<u>Page</u>
Abstract.....	1
Nomenclature.....	2
Introduction	
Background of Research.....	3
Summary of Present Investigation.....	4
Analytical Program	
Analysis for a Single-Blade Row.....	5
Fundamental Mode of Operation.....	5
Analytical Formulation.....	10
Results of Analytical Program.....	13
Comparison of Results with Monte Carlo Calculations	15
Truncation Errors in Numerical Solutions.....	16
Extension of Compressor Research.....	
Single-Row Compressor.....	18
Experimental Technique.....	20
Two-Row Compressor.....	21
Experimental Results with Single-Row Compressor....	21
Experimental Results with Two-Row Compressor.....	25
Free-Molecule Cascade Tests.....	
Apparatus.....	27
Procedure.....	28
Experimental Results with Free-Molecule Cascade....	29
Effect of Aspect Ratio.....	30
Effect of Spacing-Chord Ratio.....	31
Effect of Blade Curvature.....	32
Appendix A	
Derivation of Functions used in Analytical Solution	33
Appendix B	
Determination of $\Sigma_0$ in Cascade Tests.....	42
References.....	45

FREE-MOLECULE FLOW IN THE AXIAL-FLOW TURBO-VACUUM PUMP

by

John S. Maulbetsch and Ascher H. Shapiro

ABSTRACT

The rarefied gas flow through a moving cascade of flat plates was investigated analytically and experimentally, with the application in mind of high-vacuum pumping.

The theory is based on the assumption of free-molecule flow, i.e., no collisions between molecules. The essential quantities determining the performance of a blade row are the net transmission probabilities from one side to the other. These transmission probabilities depend mainly on the blade angle and spacing-chord ratio and on the ratio of mechanical speed to mean molecular speed. In this report the transmission coefficients are calculated by numerical solution of the governing integral equations, and are compared with the results of earlier Monte Carlo calculations.

Experiments with a rotating test machine having either a single rotor or a rotor followed by a stator gave results in good agreement with the theory.

A special means was developed for testing stationary cascades under conditions simulating the operation of a moving rotor. This apparatus was tested with several blade geometries. The results confirmed both the theory and the feasibility of the new rarefied gas wind-tunnel concept.

NOMENCLATURE

AR	Aspect ratio (blade span to width of passage between blades).
b	Blade chord.
$\bar{c}$	Average molecular speed for Maxwellian distribution, $\sqrt{8RT/\pi}$
n	Molecular number density.
$\dot{N}$	Effusion flux, number of incident molecules per unit area per unit time.
p	Pressure.
R	Universal gas constant divided by the molecular weight of the gas.
s	Blade spacing in the tangential direction.
S	Ratio of the mean mass speed of the gas, relative to the blades, to the most probable molecular speed. $S = V/\sqrt{2RT}$ .
T	Temperature.
u, v, w	Components of the thermal velocities of molecules.
V	Magnitude of the mean mass velocity of the gas relative to the blades.
$V_B$	Blade speed, in tangential direction.
$V_T$	Axial component of mean mass throughflow velocity of the gas.
W	Ho Coefficient (the <u>net</u> flux of molecules through the cascade, expressed as a fraction of the flux $\dot{N}_1$ incident on the upstream side).
$\alpha$	Blade angle with the tangential direction.
$\beta$	Angle which the mean mass throughflow velocity of the gas makes with the axial direction.
$\Sigma_{12}$	Transmission coefficient (the fraction of molecules incident on side 1 of the blade row which ultimately emerge to side 2).

The subscripts 1 and 2 refer to the upstream and downstream sides of the blade row, respectively.

## INTRODUCTION

### Background of Research

Until recently, it had always been assumed that methods used for pumping or compressing gases at the very low pressures dealt with in vacuum technology would necessarily be quite different from those normally employed at aerodynamic pressures. The expected pressure ratios per stage associated with axial-flow or centrifugal compressors operating at aerodynamic pressures are so low (1.05 to 1.2 for the axial-flow; 1.5 to 2.0 for the centrifugal) that far too many stages would apparently be required to obtain the overall pressure ratios required in high-vacuum applications. However, at very low density levels the molecular structure of the gas may no longer be ignored in considering the flow mechanism. The entire operation of fluid machinery must then be looked at from a molecular view point. The normal limitations on pressure ratio --- adverse pressure gradients, separation, shock waves, surging, and stalling --- are no longer meaningful. That large pressure ratios per stage can be achieved by axial-flow machines in the free-molecule range of pressures was demonstrated by the experiments of Becker <sup>(1)</sup> and of Hablani <sup>(2)</sup>.

The present project was initiated under sponsorship of the Office of Naval Research after approximate calculations for the case of very high blade speeds indicated the possibility of extremely high pressure ratios per stage and gave some idea of the influence of the blade row geometry. Our object has been to provide a theoretical and experimental foundation on which axial-flow bladed vacuum pumps may be designed and

their performance predicted. Initial results were presented in our first report<sup>(3)</sup> to the Office of Naval Research under this contract. These, together with some additional material, have been summarized in two published articles<sup>(4)</sup> <sup>(5)</sup>.

We present herewith our final report on the subject, constituting a definitive account of the performance of moving cascades of flat plates in the free-molecule regime.

#### Summary of Present Investigation

The work described in this report may be divided into three sections.

First, the theoretical problem has been solved by numerical solution of the governing integral equation. For single blade rows, this made it possible to extend the theory over a wider range of operating parameters, and also to eliminate the not inconsiderable statistical errors inherent in the Monte Carlo method used previously in reference 3.

The second aspect of the program was the extension and refinement of the previous experimental studies, using the existing apparatus.

The third and most novel phase of the research was the testing of free-molecule cascades in an adaptation of the device which in effect made it into a new type of low-density wind tunnel. This allowed us to test a variety of blading configurations more conveniently and rapidly than would be possible in a rotating machine. The scheme used has application to a wide variety of low-density wind-tunnel experiments.

## ANALYTICAL PROGRAM

### Analysis for a Single-Blade Row

The Monte Carlo method for calculating the molecular flows through the machine has been described fully by Kruger<sup>(3)</sup>. This method, essentially statistical, was chosen because at that time it was thought to require less machine time than the solution of the integral equations in terms of which the problem may also be formulated. This was undoubtedly the case for the multi-row calculations, for which the molecular velocity distributions are non-Maxwellian. Furthermore, the direct analogy between the individual samples of the Monte Carlo method and the individual molecules in the flow made the method look particularly attractive. In fact, for problems involving a complicated geometry, or for the precise calculation of stages in series, the statistical approach may well be the only feasible one.

However, in some cases it is preferable to solve the integral equations. For single rows of flat plates, such as are considered here, the computer time involved in the integral solution is much less than that needed for the Monte Carlo solution. Therefore, in order to cover a wide range of variables, and also to get more accurate results with the amount of machine time available, the integral equations were programmed on the IBM 7090 computer. This had the added advantage of providing certain intermediate results which might be helpful in designing better blade shapes for such varying requirements as high pressure ratio or high incident-molecule capture.

### Fundamental Mode of Operation

The operating characteristics of the machine may be understood by

considering two regions of gas, separated by a row of flat-plate blades

(Fig. 1) moving with the speed  $V_B$ . We shall make the following assumptions:

1. The upstream and downstream regions are each Maxwellian.
2. The flow is free-molecular with respect to the blade dimensions. This requires that the mean-free path of the molecules be much greater than the blade dimensions, and allows one to ignore inter-molecular collisions within the blade row.
3. The temperatures in the two regions are equal. This is justified by the consideration that the rate at which energy is carried to the blades and the casing by the molecules is small compared to the rate at which it can be conducted or radiated away.
4. A stationary state prevails.

It can be shown from molecular flow theory<sup>(6)</sup> that the number of molecules incident upon the blade row per unit area per unit time from a Maxwellian region of number density  $n$  is given by

$$\dot{N} = \frac{n \sqrt{2RT}}{2} \left[ \frac{1}{\sqrt{\pi}} e^{-x^2} + x (1 + \operatorname{erf} x) \right] \quad (\text{Eq. 1a})$$

where  $x \equiv S \cos \beta$  (Eq. 1b)

and  $\operatorname{erf} x \equiv \frac{2}{\sqrt{\pi}} \int_0^x e^{-\xi^2} d\xi$

Now let  $\Sigma_{12}$  represent the probability that a molecule incident upon the blade row from region 1 will ultimately reach region 2 (perhaps after many reflections from the blades), and  $\Sigma_{21}$  the same probability of transmission from region 2 to region 1. Then, for zero net throughflow, the number of molecules passing through the row in opposite directions must be equal:

$$\dot{N}_1 \Sigma_{12} = \dot{N}_2 \Sigma_{21} \quad (\text{Eq. 2})$$

When a net throughflow exists, we may characterize the volume flow by means of the Ho Coefficient,  $W$ , defined as the ratio of the actual molecular throughflow to the maximum possible throughflow.\* This maximum is  $\dot{N}_1$ , and therefore the requirement of conservation of molecules within the blade row leads to

$$\dot{N}_1 \Sigma_{12} - \dot{N}_2 \Sigma_{21} = \dot{N}_1 W \quad (\text{Eq. 3})$$

The effusion flux  $\dot{N}$  depends on  $S \cos \beta$  according to Eq. 1, and hence depends on the blade speed  $V_B$ , on the mean mass throughflow velocity  $V_T$ , and on the most probable thermal speed,  $\sqrt{2RT}$ . However, as we shall now show,  $S \cos \beta$  is in fact extremely small. From the geometry of Fig. 1,

$$\cos \beta = V_T / V \quad (\text{Eq. 4})$$

---

\*The Ho Coefficient is related to the net volume throughflow by the equation

$$\text{Net Volume Throughflow} = \sqrt{RT/2\pi} \cdot W$$

and, by definition,

$$S \equiv V/\sqrt{2RT} \quad (\text{Eq. 5})$$

Furthermore, since the mean mass throughflow velocity is equal to the volume flow per unit area, we may write

$$V_T = \frac{\dot{N}W}{n} K_A \quad (\text{Eq. 6})$$

where  $K_A$  is the ratio of the throughflow area at the cascade to the throughflow area a mean-free-path length away from the cascade, in the region from which the molecules are incident on the cascade. Combining Eqs. 4, 5 and 6, we form

$$x \equiv S \cos \beta = \frac{\dot{N}}{n\sqrt{2RT}} WK_A \quad (\text{Eq. 7})$$

Thus, Eq. 1a may now be written as

$$x = \frac{K_A W}{2} \left[ \frac{1}{\sqrt{\pi}} e^{-x^2} + x(1 + \text{erf } x) \right] \quad (\text{Eq. 8})$$

Expanding the functions on the right-hand side in ascending powers of  $x$ , and simplifying, we get

$$x = \frac{K_A W}{2\sqrt{\pi}} \left[ 1 + \sqrt{\pi} x + x^2 - \frac{x^4}{6} + \frac{x^6}{30} - \dots \right] \quad (\text{Eq. 9})$$

This may be inverted to give

$$\alpha = S \cos \beta = \frac{K_A W}{2\sqrt{\pi}} \left[ 1 + \frac{K_A W}{2} + \frac{\pi+1}{\pi} \left( \frac{K_A W}{2} \right)^2 + \dots \right] \quad (\text{Eq. 10})$$

Now  $W$  can never exceed unity, and, in any practical situation, it is likely to be not more than  $1/2$ . In our experiments with the one-row compressor (single rotor) and with the two-row compressor (single rotor followed by single stator),  $K_A$  was equal to  $0.274$ . Hence  $S \cos \beta$  was at most equal to about  $0.04$ , and was generally far less. In our experiments with the stationary cascade apparatus,  $S \cos \beta$  was always less than  $.035$ .

The foregoing analysis shows that for most purposes it is sufficient to assume that  $S \cos \beta \cong 0$ . With this assumption it follows from Eq. 1 that

$$\dot{N} \cong \frac{n \sqrt{2RT}}{2\sqrt{\pi}} = \frac{n \bar{c}}{4} \quad (\text{Eq. 11})$$

Then, since the temperatures are the same in regions 1 and 2, Eq. 3 may be put in the following form which expresses the operating performance of the row insofar as it relates the pressure ratio  $n_2/n_1$  across the row to the volume throughflow parameter  $W$ :

$$\frac{n_2}{n_1} = \frac{\Sigma_{12}}{\Sigma_{21}} - \frac{W}{\Sigma_{21}} \quad (\text{Eq. 12})$$

Since, as shown above, the net throughflow imparts only a very small mean mass velocity to the gas in the axial direction, the  $\Sigma_{1A}$  are only weak functions of  $W$ . Neglecting this dependence, the analytical problem reduces to that of determining the values of  $\Sigma_{12}$  and  $\Sigma_{21}$  as functions of the dimensionless blade speed  $S = V_B / \sqrt{2RT}$  and the blading parameters  $\alpha$  and  $s/b$ . Note that in the free-molecule range, the absolute density level and the Knudsen number are not significant variables.

#### Analytical Formulation

The problem may be divided into two parts: (1) the determination of the initial incidence distribution of molecules from the Maxwellian regions as they arrive at the blade surfaces; and (2) the evaluation of the ultimate transmission probabilities for molecules within the blade row after they have been emitted from one of the blade surfaces. The analysis is illustrated by Fig. 2.

The fraction  $\sigma_{12}$  of molecules incident upon the blade row from region 1 which pass directly to region 2 without colliding with a blade surface can be computed explicitly in terms of the variables  $\alpha$ ,  $s/b$ ,  $\beta$  and  $S$ .

Next, the fraction of incident molecules which impinge directly upon the blade area  $d\alpha$  at position  $x$  (or  $dy$  at  $y$ ) along the surfaces of the blades may be calculated, in terms of the so-called initial incidence distribution. These are characterized by the density distribution functions  $\nu_x$  and  $\nu_y$ , such that  $\nu_x d\alpha$  is the fraction of all molecules entering the passage from region 1 which impinge directly on the area  $d\alpha$ , and similarly for  $\nu_y dy$ .

Now let  $\tau_{x2}$  be the ultimate probability of a molecule's reaching region 2 after having been emitted from area  $dx$  at  $x$  (after, perhaps, a number of collisions with the blade surfaces), and let  $\tau_{y2}$  be similarly defined. Then the overall transmission coefficient,  $\Sigma_{12}$ , may be expressed as

$$\Sigma_{12} = \tau_{12} + \int \nu_x \tau_{x2} dx + \int \nu_y \tau_{y2} dy \quad (\text{Eq. 13})$$

where it is to be understood that the integrations are over the entire length of each blade.

In this expression all quantities may be calculated directly from the known quantities except for the functions  $\tau_{x2}(x)$  and  $\tau_{y2}(y)$ . For this calculation, consider molecules being emitted from a  $dx$  at  $x$  on the left-hand blade surface. Let us define  $C_{x2}$  as the fraction which passes directly from  $dx$  to region 2 without collision, and  $F(x,y) dy$  as the fraction which passes directly from  $dx$  to some  $dy$  at  $y$ . Then, since the rate of molecular incidence on any area equals the rate of molecular emission, we may write

$$\tau_{x2} = C_{x2} + \int \tau_{y2} F(x,y) dy \quad (\text{Eq. 14a})$$

and, similarly,

$$\tau_{y2} = C_{y2} + \int \tau_{x2} F(y,x) dx \quad (\text{Eq. 14b})$$

In this pair of simultaneous integral equations, the functions  $C_{x_2}(x)$ ,  $C_{y_2}(y)$ ,  $F(x, y)$ , and  $F(y, x)$  may be computed from the geometry of the blading and the cosine law for diffuse reflection. They are independent of the speed of the blade row. When the cosine law is valid, it may be further shown that  $F(y, x) = F(x, y)$ .

For the special case of flat plate blades, with which we are dealing, certain conditions of symmetry prevail, greatly simplifying the problem. These are that, at equal values of  $x$  and  $y$ ,

$$\sigma_{x_2} = \sigma_{y_1} \quad ; \quad \sigma_{x_1} = \sigma_{y_2} \quad (\text{Eq. 15})$$

Moreover, these four values of  $\sigma$  must satisfy the conservation relations

$$\sigma_{x_1} + \sigma_{x_2} = \sigma_{y_1} + \sigma_{y_2} = 1 \quad (\text{Eq. 16})$$

Using Eqs. 15 and 16, Eqs. 14a and 14b may be combined and reduced to

$$\sigma_{y_2} = (1 - C_{y_1}) - \int \sigma_{y_2} F(x, y) dy \quad (\text{Eq. 17})$$

To solve this equation, the integral on the right-hand side was first expressed as a sum of twenty terms, based on the trapezoidal rule for numerical quadrature. Then the function  $\sigma_{y_2}(y)$  was solved for by iteration. This in turn gave  $\sigma_{x_2}(x)$ , and then Eq. 13 could be solved for  $\Sigma_{12}$ .

The analytical expressions for all the functions defined above are to be found in Appendix A. The functions were computed, and Eqs.

17 and 13 solved, on the IBM 7090 computer at the M.I.T. Computation Center, using numerical quadrature with twenty intervals for each integral.

### Results of Analytical Program

The results of the calculation program for flat-plate arrays have been collected and exhibited in several ways:

1. In Table 1 are displayed the values of  $\Sigma$  for systematic variations of the geometric parameters  $\alpha$  and  $s/b$  and of the blade-speed parameter  $S$ . Note that these are all based on the assumption  $S \cos \beta \cong 0$ . Note further that positive values of  $S$  correspond to  $\Sigma_{12}$ , while negative values of  $S$  correspond to  $\Sigma_{21}$ .
2. Figures 3, 4, 5, 6, and 7 show the same information graphically.
3. Figures 8, 9, 10, 11, and 12 show the two combinations of the  $\Sigma$ 's which are indicative of the performance of the machine. Note, from Eq. 12, that  $\Sigma_{12}/\Sigma_{21}$  gives the pressure ratio for zero throughflow, while  $\Sigma_{12} - \Sigma_{21}$  gives the value of  $W$  for no pressure rise.
4. Figures 13, 14, and 15 are cross-plots of Figures 8 through 12, showing the effect of spacing-chord ratio on  $\Sigma_{12}/\Sigma_{21}$  and  $\Sigma_{12} - \Sigma_{21}$ .
5. Figures 16, 17, and 18 are similar cross-plots, showing the effects of blade angle  $\alpha$ .
6. Figures 19 and 20 show certain intermediate information regarding the incident flux distributions,  $\psi_x$  and  $\psi_y$ , and the ultimate transmission probability,  $\sigma_{xz}$ , of molecules reflected from the blade surfaces.

In examining the results of the analysis, one must do so in the light of the characteristics of operation that would be required of the individual blade rows in an actual compressor. Equation 12 shows that, for high pressure ratio per stage, the ratio  $\Sigma_{12} / \Sigma_{21}$  should be large, while for large pumping capacity, the difference  $\Sigma_{12} - \Sigma_{21}$  should be large. These goals are generally not compatible. For instance, the highest pressure ratios are attained with  $\alpha = 10^\circ$  or  $20^\circ$  and with  $s/b = 1/4$  or  $1/2$ . However, these configurations have low values of the throughflow parameter  $\Sigma_{12} - \Sigma_{21}$ .

However, practical consideration of a working design for such a compressor indicates that the situation is not necessarily an unfortunate one. In considering the requirements for high-vacuum technology, one normally thinks in terms of absolute pressure levels of  $10^{-8}$  to  $10^{-3}$  mm Hg. or lower. If a compressor, such as the one under discussion, were to be used to attain such a pressure level, it would probably be operated in conjunction with a mechanical forepump with a blank-off pressure of, at best,  $10\mu$  ( $10^{-2}$  mm Hg.). This would require a pressure ratio across the machine of approximately  $10^6$  or more. Such a pressure ratio clearly cannot be obtained with a single blade row. Operating in air, (with a most probable molecular speed at  $68^\circ\text{F}$  of approximately 1350 ft/sec.), the best blade-speed ratio one could hope to attain is about unity. Even at zero flow this would require at least six or seven stages. At a zero-flow condition, the most efficient design would clearly be one which incorporated identical stages all providing the highest possible pressure ratio. However, since even at "blank-off" there is always a net throughflow, and since one must pass through a "pump-down" period, high volume flow is actually as important for the machine as a whole as high pressure ratio.

Now the mass throughflow is the same for all stages of a multi-stage machine, and thus the volume throughflow is inversely proportional to the pressure level upstream of each row. Hence, for a multi-stage machine, all the stages need not perform the same function. The stages near the outlet, where the pressure level is relatively high, should provide high pressure ratios per stage. For in this region the  $H_0$  coefficient is nearly zero. Near the low-pressure end, on the other hand, where the volume throughflow is likely to be quite large, blade configurations should be chosen to accommodate high flow and still provide some reasonable pressure ratio. Thus, closely-spaced blades with small blade angles are desirable near the high-pressure end of the machine, while more widely spaced blades with larger angles are desirable for the low-pressure end of the machine.

#### Comparison with Results of Monte Carlo Calculations

It is of interest to compare the computed results presented here with the corresponding statistical results obtained by the Monte Carlo method<sup>(3)</sup>. There are 81 cases exactly comparable with respect to the values of  $\alpha$ ,  $s/b$ , and  $S$ .

The two sets of results for these 81 cases can only be compared on a statistical basis. Accordingly, the percent error for the Monte Carlo calculation was calculated for each of the 81 cases, on the assumption that the present results are, in fact, correct. These cases were then arranged in ascending order of error, from the largest negative error to the largest positive error. The errors were then plotted (Figure 21a) in the form of the integral of an error distribution

function: i.e., the fraction of the total cases with an error less than a given error was plotted against the given error. The smoothed integral curve of Fig. 21a was then differentiated to give the error distribution function of Fig. 21b.

On the assumption that the result of a Monte Carlo calculation would be normally distributed around the correct answer, the number of samples used was approximately chosen such that there would be only a 10.96% probability that any particular result would be in error by more than 10%. This is sufficient information to construct the theoretical error distribution function from standard probability tables. The normal distribution function for the "expected" standard deviation of  $\sigma = 0.0625$  is shown in Fig. 21b.

The actual error distribution and the "expected" distribution, as exhibited in Fig. 21b, are in general agreement, to the extent of giving credence to both the Monte Carlo results and to the present results. That value of the fractional error, with respect to which half the errors are greater and half less, is about  $-1/2\%$ , which seems quite reasonable for a sample of 81 cases. This comparison of the means may be associated with the small truncation error of the integral calculations, as described below, but this is somewhat speculative.

The important conclusion to be drawn from Figure 21 is that both the Monte Carlo results and the present results, reached by completely different calculation routes, are in substantial agreement. The implication is that both are substantially correct. We believe, however, that the present results are the more reliable in individual cases.

#### Truncation Errors in Numerical Solution

In order to investigate whether a division of each blade surface into twenty zones for purposes of numerical quadrature of the integrals

in Eqs. 13 and 17 was sufficient, trial calculations were also made for ten, forty, and eighty zones. From these trials it appears that the truncation error is less than 1/2% .

EXTENSION OF COMPRESSOR RESEARCH

The second phase of the investigation involved the refinement of the experimental program on the single-row compressor with  $\alpha = 20^\circ$ ,  $s/b = 0.46$ , and an extension to a two-row machine comprising a rotor and stator having mirror-image geometries.

Single-Row Compressor

The experimental work was performed on the existing apparatus. A cross-sectional layout of the machine is shown in Fig. 22. Figure 23 is a schematic of the associated equipment and instrumentation. Although a description of the apparatus and the experimental technique appears in our first report<sup>(3)</sup>, it is repeated here for the convenience of the reader.

The test section consisted of a cylindrical steel housing in which the aluminum compressor rotor was driven by a high-frequency induction motor. To maintain densities sufficiently low for free-molecule flow in the test section, the housing was mounted directly on a six-inch oil diffusion pump with its axis, and the axis of the compressor rotor, in a vertical direction. The shaft connection between the rotor and the induction motor was made through an annular clearance seal 0.750 inches in diameter, 0.540 inches in length, and with a radial clearance of .002 inches. Using the formula for a thin slitlike tube, the molecular conductance of the clearance seal is found to be  $1.13 \times 10^{-3}$  liters per second for air at  $20^\circ\text{C}$ . Thus, if the pressure on the motor side of the seal is maintained at a micron or less, the flow from the region

of the motor is of the order of  $10^{-3}$  micron-liters per second, a negligible leak at the conditions of the tests. To ensure this condition, the motor housing was connected to a two-inch oil diffusion pump. As a further precaution, a low vapor-pressure silicone grease was used as a lubricant for the motor ball bearings. Provision was made to admit gas to the system both above and below the rotor. Seals between the system and the atmosphere were maintained by means of welded and soldered joints, O-rings, special gasket seals for the ionization gauges, and, in the case of the thermocouple gauges and the gas inlet tubes, by red glyptal lacquer.

The densities upstream and downstream of the compressor rotor were measured by hot filament ionization gauges. One thermocouple gauge was used to insure that the pressure in the motor housing was below one micron, and another was connected to the test section upstream of the disk. The flow rate of gas admitted into the system was measured on the high-pressure side of the leak valve by the displacement of a column of mercury in essentially the same manner as that described by Dushman.<sup>(7)</sup> It was assumed that the mass flow rate of gas through the leak valve was proportional to the square of the pressure on the high pressure side of the valve, as for compressible flow at low Reynolds numbers, and the flow measurement was used to determine this constant of proportionality. The speed of the rotor was measured by a permanent magnet-and-coil tachometer and an electronic counter. The temperature of the outer race of the bearing at the rotor end of the shaft was monitored with a thermocouple and potentiometer.

### Experimental Technique

The apparatus was prepared for testing by thoroughly cleaning all surfaces to be exposed to the vacuum with acetone and by heating the entire apparatus with infrared lamps to a temperature of the order of 100°C for several hours with the vacuum pumps operating. At zero blade speed, with both leak valves closed, a pressure of about  $2 \times 10^{-6}$  mm Hg was obtained at the downstream ionization gauge. A comparison of this value with the reading of the upstream ionization gauge gave an approximate value for the flow rate from leaks and virtual leaks in the system, using the single-blade-row calculations for a stationary rotor to determine its impedance to gas flow. Since the density ratio across a rotating blade row is a function of the upstream volume flow rate, the effect of these small leaks in the system was made negligible by admitting gas through the downstream leak valve and raising the density level in the system. Tests were conducted at density levels for which no density drop was measurable across the stationary rotor.

The dimensions of the compressor rotor used are given in Fig. 22. Angular velocities in the range from 20,000 to 30,000 r.p.m. gave tip speeds from 620 to 955 feet per second. Ordinary air was used as the test gas for the compressor tests. In the cascade experiments, described later, xenon was also used because its lower molecular speed allowed higher dimensionless blade speeds to be reached. The pressure downstream of the rotor was maintained at about  $10^{-4}$  mm Hg by means of the lower leak valve. The flow of gas through the rotor was controlled by the upper leak valve and the flow rate was measured by the displacement of a mercury column, as previously described, and by the density drop across

the compressor rotor at zero blade speed.

#### Two-Row Compressor

The two-row compressor was built as a combination of the rotor previously described and of a following stator having a geometry that was a mirror image of that of the rotor. Figure 24 shows details of the arrangement and gives pertinent dimensions.

The spacing between two rows was made as small as possible in order to minimize the effects of the end walls, and also to reduce the size of the annular passage designated by  $L$  in Fig. 24. This annulus represents a leakage path through which molecules from the high density side may bypass the stator with a transmission probability of nearly unity. However, this throughflow area was negligibly small in comparison to the throughflow area of the stator, and thus its effect on the performance of the machine was also negligible.

#### Experimental Results with Single-Row Compressor

On Figures 25, 26, and 27 are displayed the experimental data and calculated results for the single-row rotating machine, with air as the test gas.

The pressure ratio across the rotor, for zero net throughflow, is shown in Fig. 25. Also shown are the experimental data of Kruger and Shapiro<sup>(4) & (5)</sup>, as well as the theoretical pressure ratio for zero throughflow, as computed from Eq. 12 and the transmission coefficients of Table 1. It is to be noted that the blade speed  $S$  in the abscissa of Fig. 25 is reckoned at the arithmetic mean radius between the

tip radius of the blades and hub radius; correspondingly, the value of  $s/b = .46$  is also reckoned at the same mean radius. The present results and the earlier data of Kruger and Shapiro are in agreement to within the accuracy of measuring the pressures.

While the theoretical predictions are in general agreement with the experimental results, and while they certainly follow the same sort of curve, there is a substantial discrepancy, with the experimental rotor showing distinctly better performance than would be anticipated from the theoretical calculations. For instance, at a blade-speed ratio of 0.50, the theoretical expectation of zero-throughflow pressure ratio is about 2.85, whereas the measured pressure ratio for zero throughflow is about 3.75.

Fig. 26 shows, for several different values of the dimensionless speed ratio  $\hat{S}$ , the measured curves of pressure ratio across the row against volume throughflow. The latter is expressed in terms of the volume throughflow parameter  $W$ , namely, the ratio of the actual volume throughflow to the volume throughflow incident on the blade row from the upstream end. The ordinates of Fig. 26 have been normalized with respect to the pressure ratio for zero throughflow. In other words, they represent the pressure ratio for a given volume throughflow to the pressure ratio corresponding to zero throughflow for the same  $\hat{S}$ , as displayed on Fig. 25. According to Eq. 12, the curves of density ratio vs. volume throughflow should be straight lines, at least for the limiting case  $\hat{S} \cos \beta = 0$ . It may be noted from Fig. 26 that the experimental data do indeed follow straight lines within the experimental accuracy.

Referring again to Eq. 12, the experimental values of the

transmission coefficients  $\Sigma_{12}$  and  $\Sigma_{21}$  may be calculated from the intercepts of the straight line of pressure ratio vs. volume flow. Thus, using the experimental data of Fig. 25 and the "best" straight lines of Fig. 26, the transmission coefficients were calculated as a function of the dimensionless speed ratio  $\hat{S}$ . The results are shown in Fig. 27. Also shown on Fig. 27 is the theoretical curve of transmission coefficient vs. dimensionless speed ratio, as interpolated from Table 1.

The experimental data in Fig. 27 are in general agreement with the theoretical predictions. For positive values of  $\hat{S}$ , the measured transmission coefficients lie higher than the theoretical; for negative values of  $\hat{S}$ , they lie slightly lower.

All the experimental results for the single-row rotating machine are essentially summarized in Fig. 27, and it remains now to inquire as to the possible sources of discrepancy between the measured values of transmission coefficient and the theoretical. To the degree that the actual conditions of the experiment duplicated the postulates of the theoretical model, we should expect substantially perfect agreement. However, there were several deviations, and these will now be discussed and their significance appraised:

1. The molecular fluxes incident on the rotor from the upstream and downstream sides were not necessarily exactly Maxwellian. However, the mode of operation of the moving cascade is such that slight departures from Maxwellian conditions should not have much effect on the transmission coefficients. Accordingly, this is not felt to be a significant source of deviation between theory and experiment.

2. Earlier, in connection with Eq. 1, and in the calculations of  $\Sigma_{12}$  and  $\Sigma_{21}$ , the theoretical calculations were simplified by assuming that  $S \cos \beta$  is approximately zero. This is not exactly correct. Estimates of the amount of error this might involve, however, indicate that this approximation could scarcely be the source of the difference between theory and experiment observed in Fig. 27.
3. In making the theoretical calculations, it was assumed that molecules incident on the blades would be reflected in a diffuse manner. That is, the molecules emitted from the surface were calculated as though they came from a Maxwellian region behind the surface. Examination of the geometry of the blade rows shows that even a very small proportion of specular rather than diffuse reflection would make an enormous difference in the transmission coefficients. In particular, it would greatly increase the transmission coefficient  $\Sigma_{12}$ , and it would greatly decrease the transmission coefficient  $\Sigma_{21}$ . We have nothing firm on which to judge whether this was a significant factor, but a comparison of these results with those of the two-row rotating machine and with those for the stationary cascade suggests that this was not the essential source of discrepancy.
4. The most likely source of discrepancy between theory and experiment in Fig. 27, especially when we take into account the experimental and theoretical comparisons for the two-row rotating machine and the stationary cascades, is the fact that the cascade is not strictly two-dimensional. Entirely apart from the variation of radius and of blade speed along the span of the blades, the most important factor seems to be that in the actual machine there are end walls

to the cascade. One of these end walls, at the hub, is stationary with respect to the blades. The other end wall, at the casing, is moving with respect to the blades. The stationary end wall tends to reduce the values of both transmission coefficients,  $\Sigma_{12}$  and  $\Sigma_{21}$ , through what may be thought of as a frictional resistance. If one examines the relationship between the moving end wall and the blades, it will be seen that any molecules incident upon this moving end wall will be reflected back into the blade row in such a way as to improve their chances of being emitted toward the downstream side. This tends to increase the value of  $\Sigma_{12}$  and to decrease the value of  $\Sigma_{21}$ , a trend in agreement with the comparison of Fig. 27. Moreover, as further indication that this may well be the principal explanation, note that at a value of the dimensionless blade speed ratio  $S = 0$ , where the effect of the moving end wall would be minimized, the agreement between theory and experiment is within the accuracy of the experimental data. As further evidence on this point, the effect of the stationary end walls at  $S = 0$ , according to the investigations described later with stationary cascades having various aspect ratios, is quite small.

#### Experimental Results with Two-Row Compressor

Figs. 28, 29, and 30 show the experimental data and the computed experimental results for the two-row rotating machine. These three figures are comparable in their construction to Figs. 25, 26, and 27 respectively, and may be interpreted in the same way. The one point requiring clarification has to do with the theoretical calculation of

the transmission coefficients shown in Fig. 30. These were calculated from the single-row transmission coefficients of Table 1 using the calculation procedure described in ref. 5. Note further that the solid curve of Fig. 28 is the overall zero-flow density ratio, while the dashed curve is the zero-flow density ratio for the stator alone, found by combining the results of Fig. 25 with the solid curve of Fig. 28.

In assessing the comparison between the experimental and theoretical results for the two-row rotating machine, we may restate the first three comments made above with respect to the similar comparison for the single-row rotating machine. The last comment made above, however, requires modification, inasmuch as the stator of the two-row machine had two stationary end walls. This would have the result of reducing the transmission coefficients  $\Sigma_{12}$  and  $\Sigma_{21}$  for the stator row. This interpretation, when applied to the one-row machine (Figs. 25, 26, and 27) and to the two-row machine (Figs. 28, 29 and 30), seems to make for a consistent picture, especially when it is realized that there is a leakage backflow around the stator.

### FREE-MOLECULE CASCADE TESTS

The third stage of the program represented the most novel contribution of the present research. Its purpose was two-fold. The first was to enlarge the scope of existing experimental results applicable to the free-molecule compressor by testing a variety of different blade geometries. The second was to test a new concept in low-density "wind tunnels". To obtain the required data through the use of rotating blade rows would have necessitated the building and balancing of a new rotor for each geometry tested. The alternative scheme was based on a free-molecule cascade in which a mean mass velocity was imparted to the gas on one side of a stationary blade row by means of an unbladed rotor.

#### Apparatus

An assembly drawing of the apparatus, modified for use as a cascade wind-tunnel, is shown in Fig. 31a.

The blades were mounted in one quadrant of the cylindrical shell separating zones 1 and 4, as shown in Fig. 31b. Since the blades in this arrangement are stationary, there is no problem of strength or balancing. They were simply cut out of thin sheet-stock brass with tin snips, and were held in place in the blade racks with small dabs of epoxy resin at each corner. A mean mass velocity was imparted to the incident molecules on one side of the cascade by the high-speed rotor. The design of the outer edge of the rotor, with two small ridges on the top and bottom, insured that all molecules incident on the blade row from region 1 were emitted from the outer edge of the rotor. Therefore,

under the assumption of diffuse reflection, the gas in region 3 had a mean mass velocity with respect to the blade row equal to the peripheral speed of the rotor. Thus the stream of molecules emitted from the rotor played the same role as the high speed gas stream in a rarefied-gas wind tunnel.

### Procedure

In order to determine the transmission coefficients, three sets of measurements were required. The first was a calibration of the blade row as a flow-meter with the rotor locked, and with the positive displacement flowmeter used for determining  $\Sigma_0$ , the transmission coefficient of the blade row at a blade-speed ratio of zero. The second was a series of measurements of the pressure ratio across the blade row at finite blade speeds and zero net throughflow, for the determination of  $\Sigma_{12}/\Sigma_0$  vs.  $\delta$ . And the third was another set of runs similar to the second, with the blades facing in the opposite direction, to determine  $\Sigma_{21}/\Sigma_0$  vs.  $\delta$ . In the case of flat-plate blades with their accompanying symmetry, it was possible to make the third set of measurements simply by reversing the direction of rotation of the rotor.

In the original design of the apparatus, it had been intended that the resistance to flow between regions 3 and 4 and also between 4 and 5 would be negligible in comparison to the resistance of the blade row itself. This was indeed the situation in the latter case, as indicated by the fact that the pressures in regions 4 and 5 were equal. Accordingly, one could speak meaningfully of a single downstream

pressure during the determination of  $\Sigma_0$ . However, the resistance between 3 and 4 was larger than had been anticipated. This difficulty was overcome by measuring two resistances; first, that without the blades present; and, second, that with the blades in place. From these two pieces of information it was possible to evaluate the resistance of the blade row alone. The method is described in Appendix B.

The experimental technique was essentially the same as that described for the single-stage compressor, with one addition. As mentioned earlier, it was necessary that the pressures in regions 4 and 5 be identical in order that the downstream pressure be a unique quantity. To this end a large passage was provided around the rotor between the regions, but an additional ionization gauge was installed for region 4 and monitored during the tests to insure that such equality existed. This problem of flow resistance between the various regions was, of course, a matter of concern only in the calibration test for determining  $\Sigma_0$ . The tests at finite blade speed to determine the plot of zero-flow density ratio vs. blade speed ratio were conducted with no throughflow. At this condition the resistance to net throughflow between the three regions is of no concern.

#### Experimental Results with Free-Molecule Cascade

The experiments performed had three main goals:

1. To check out the theory for a variety of flat-plate blade geometries without the necessity of machining new rotors for each case.
2. To investigate the influence of end-wall effects, in terms of the aspect ratio as an experimental parameter.

3. To test non-flat-plate blade shapes for which an analysis could not readily be performed.

All the experimental data, and the associated results, are shown in Figures 32 through Figure 41.

Fig. 32 shows the curve of pressure ratio vs. throughflow for the apparatus with no cascade installed. These data were employed as indicated in Appendix B.

With the exception of Figure 36, all the other Figures are arranged in three parts, and each Figure relates to an individual blading geometry, that is, to a particular angle  $\alpha$ , solidity  $s/b$ , and aspect ratio AR. Referring to Fig. 33 as an example, ( $\alpha = 20^\circ$ ,  $s/b = 1/2$ ,  $AR = 3/2$ ), Fig. 33a shows the curve of pressure ratio vs. throughflow with the rotor locked, i.e., for  $S = 0$ . In conjunction with the data of Fig. 32, this led to the value of  $\Sigma_0$  according to the method of Appendix B. Fig. 33b shows, for zero throughflow, the curve of density ratio vs. blade-speed ratio; it was found by multiplying together the measured values of  $\Sigma_{12} / \Sigma_0$  and  $\Sigma_0 / \Sigma_{21}$ . The latter, which were of course measured individually, may be combined with the values of  $\Sigma_0$  obtained previously to give the final values of  $\Sigma_{12}$  and  $\Sigma_{21}$ , displayed in Fig. 33c.

#### Effect of Aspect Ratio

Figures 33, 34 and 35 all refer to the blading parameters  $\alpha = 20^\circ$ ,  $s/b = 1/2$ , which is very close to the corresponding parameters for the tests with the one-row and two-row rotating machines. They differ in that they pertain respectively to aspect ratios of 1.5, 2.8, and 4.0. Note, by way of comparison, that for the rotating-machine tests the aspect

ratio was about 2.4.

The most interesting feature of this series of three figures is the question of how the stationary end walls of the cascade affect the transmission coefficient. For convenience, the mean experimental curves are collected in Fig. 36, where the theoretical curve is also shown. It is evident that the transmission coefficients for an aspect ratio of 4 lie nearly at the asymptotic value for an aspect ratio of infinity, and that even for an aspect ratio of 2.5 the effect of the end walls is not very large. The theoretical results for infinite aspect ratio are, within experimental error, coincident with the experimental results for aspect ratio 4. All this tends to confirm our earlier appraisal that the main reason for the discrepancy between theory and experiment in the rotating-machine tests was the pumping effect of the moving end wall.

The effect of aspect ratio observed here is much the same as that reported in reference 8, where the results for chevron baffles with an aspect ratio of 5 were nearly coincident with those for an aspect ratio of infinity.

#### Effect of Spacing-Chord Ratio

Figures 35, 37, 38, and 39 are all for a blading angle  $\alpha = 20^\circ$  and with an aspect ratio large enough ( $>4$ ) to be considered nearly infinite. They differ in that each is for a different spacing-chord ratio,  $s/b$ , covering the range from  $1/4$  to  $3/2$ . In every case the measured transmission coefficients are in close agreement with the theoretical values.

Effect of Blade Curvature

Figures 40 and 41 show experimental data for cambered blading, for which no theoretical results are available. Each of the two cambered design is based on a straight-chord line with  $\alpha = 20^\circ$ ,  $s/b = 1/2$ , and the results are therefore to be compared with those in Fig. 35.

With the camber of Fig. 40, both the zero-flow pressure ratio and the volume-flow capacity are less than with straight blades having the same  $\alpha$  and  $s/b$ . Therefore this direction of camber is undesirable, at least in the range of  $\alpha$ ,  $s/b$ , and camber of the tests.

With the opposite camber, Fig. 41, the zero-flow pressure ratio is slightly larger than that for flat plates, but the through-flow capacity is only about half as large. Therefore this direction and amount of camber also seems to offer no substantial advantage.

APPENDIX A

DERIVATION OF FUNCTIONS USED IN ANALYTICAL SOLUTION

Initial Incidence Distributions

As explained earlier, the analytical solution may be broken up into two major steps, the first of which is the calculation of the so-called initial incidence distribution. By reference to Fig. A-1, it is seen that molecules impinging upon the blade row from region 1 may suffer one of three fates. They will either pass directly through the blade row without a collision with the surfaces and thus be of no further interest, or else they will collide with one of the two surfaces. The items of importance in this stage of the calculation are: first, the fraction which pass through the row directly, which we call  $\sigma_{12}$ ; and second, the fractions which collide with areas  $dx$  and  $dy$  on the blade surfaces at varying  $x$  and  $y$  along the blades. These distribution functions will be called  $v'_x$  and  $v'_y$ , as shown.

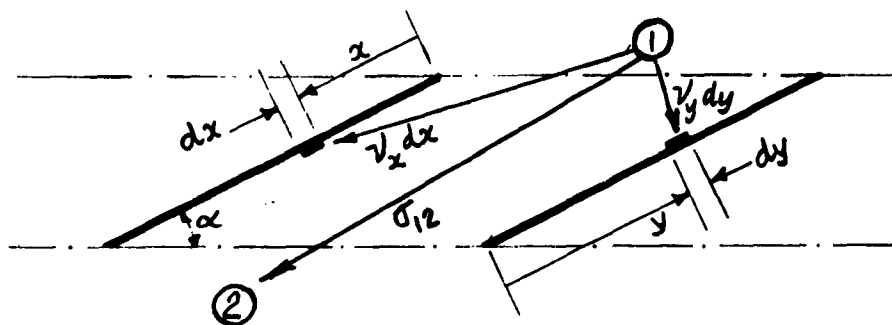


Fig. A-1

This problem will be approached, in the notation of Fig. A-2,

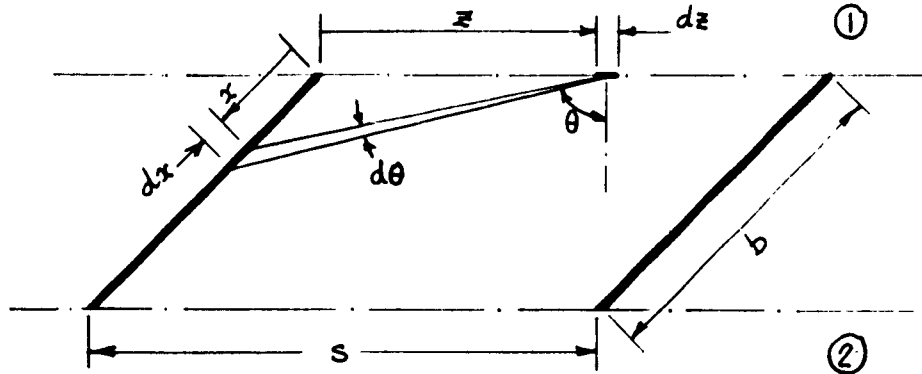


Fig. A-2

by first calculating the number of molecules incident upon area  $dx$  at  $x$  which enter the blade row by crossing the area  $dz$  at  $z$ , and then integrating across the opening between the blades from  $z=0$  to  $z=s$ . Since the incoming molecules are uniformly distributed in space, every  $dz$  has the same molecular flux. Therefore the problem is to determine for a given blade speed, what fraction of molecules crossing  $dz$  are contained in the plane angle  $d\theta$  inclined at the angle  $\theta$  to the normal. A knowledge of the blade geometry will then relate the  $x$ ,  $z$ , and,  $\theta$ , thus enabling one, at least in principle, to perform the necessary integrations.

From the point of view of an observer on the blade row, the molecules incident upon the row from region 1 will have a Maxwellian velocity distribution superposed on a mean mass velocity vector, specified by  $V$  and  $\beta$  in Fig. A-3. Let  $u$  represent the molecular velocity component along  $\xi$ ,  $v$  along  $\eta$ , and  $w$  along  $\zeta$  (normal to paper).

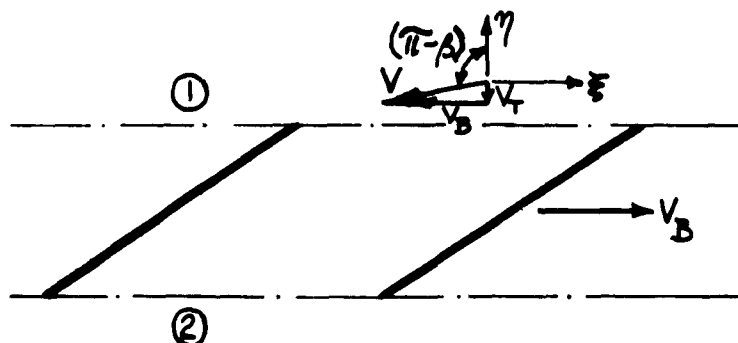


Fig. A-3

Hence the number of molecules per unit volume having velocity components lying between  $u$  and  $u + du$ ,  $v$  and  $v + dv$ , and  $w$  and  $w + dw$  is given by<sup>(9)</sup>

$$n \left( \frac{1}{2\pi RT} \right)^{3/2} e^{-\frac{1}{2RT} [(u - V \cos \alpha)^2 + (v - V \sin \alpha)^2 + w^2]} du dv dw \quad (\text{Eq. A-1})$$

Transforming from cartesian velocity coordinates  $u, v, w$  to cylindrical coordinates  $U, \theta$ , and  $w$ , according to the relations

$$u = U \cos \theta \quad (\text{Eq. A-2a})$$

$$v = U \sin \theta \quad (\text{Eq. A-2b})$$

$$w = w \quad (\text{Eq. A-2c})$$

the volume in velocity space  $du dv dw$  becomes  $U dU d\theta dw$  and

Eq. A-1 becomes

$$n \left( \frac{1}{2\pi RT} \right)^{3/2} e^{-\frac{1}{2RT} [(U \cos \theta - V \cos \alpha)^2 + (U \sin \theta - V \sin \alpha)^2 + w^2]} U dU d\theta dw \quad (\text{Eq. A-3})$$

Now, all the molecules which cross a surface per unit area per unit time with velocities between  $U$  and  $U+dU$  in the angle  $d\theta$  at angle  $\theta$  to the normal must have come from an imaginary cylinder behind the surface with slant height  $\sqrt{U^2+w^2}$  and altitude  $U \cos \theta$ . Thus the number of these molecules crossing unit surface per unit time is given by

$$\frac{n}{(2\pi RT)^{3/2}} e^{-\frac{1}{2RT}[(U \cos \theta - V \cos \beta)^2 + (U \sin \theta - V \sin \beta)^2 + w^2]} U^2 \cos \theta dU d\theta dw \quad (\text{Eq. A-4})$$

If this is now integrated with respect to  $w$  from  $-\infty$  to  $+\infty$ , and with respect to  $U$  from  $0$  to  $\infty$ , we obtain the total number of molecules crossing the surface per unit time and per unit area with velocity vectors lying in  $d\theta$  at  $\theta$ :

$$\frac{n\sqrt{2RT}}{2\pi} \left[ (1 + \text{erf } S_1) \sqrt{\pi} \left( \frac{1}{2} + S_1^2 \right) e^{-S_2^2} + S_1 e^{-S^2} \right] \cos \theta d\theta \quad (\text{Eq. A-5})$$

where

$$\begin{aligned} S &\equiv V/\sqrt{2RT} \\ S_1 &\equiv S \cos(\theta - \beta) \\ S_2 &\equiv S \sin(\theta - \beta) \end{aligned} \quad (\text{Eq. A-6})$$

Dividing now by the total flux of molecules crossing the plane to get the fraction of the total with velocities lying in  $d\theta$  at  $\theta$ , one obtains

$$\left[ \frac{(S_1/\sqrt{\pi}) e^{-S^2} + (1 + \text{erf } S_1) \left( \frac{1}{2} + S_1^2 \right) e^{-S_2^2}}{e^{-S^2 \cos^2 \beta} + \sqrt{\pi} S \cos \beta [1 + \text{erf}(S \cos \beta)]} \right] \cos \theta d\theta \quad (\text{Eq. A-7})$$

If now, both the blade surfaces and the opening between the blades are broken up into a finite number of sections as shown in Fig. A-4, the angle subtended by the  $j$ th small area  $dx$  from a point  $z$  in the center of the  $i$ th interval  $dz$  is denoted by

$$\Delta\theta_{i,j} = \theta_{i,j} - \theta_{i,j+1}$$

Where, in general

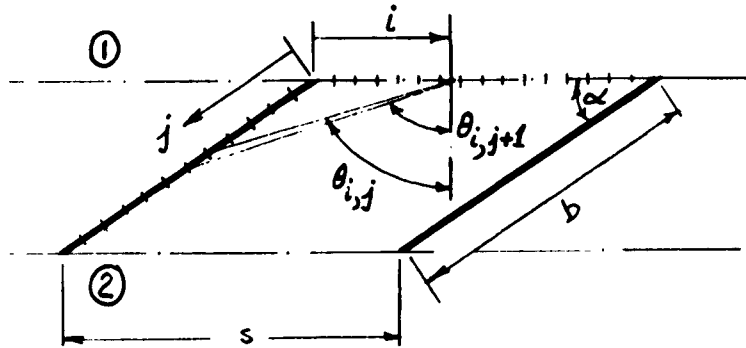


Fig. A-4

$$\theta = \tan^{-1} \left[ \frac{(s/b)(z/s) + (x/b)\cos\alpha}{(x/b)\sin\alpha} \right] \quad (\text{Eq. A-8})$$

Using Eqs. A-8, Eq. A-7 may be integrated between  $\theta_{i,j}$  and  $\theta_{i,j+1}$  for a fixed position  $i$  on the scale of  $z$ . One may then sum over all the  $i$  sections of the opening between the blades in order to obtain the total fraction of molecules from the region considered which are directly incident upon  $dx_j$ . Having done this for all  $dx_s$  and  $dy_s$ 's, one has a stepwise approximation to  $\nu_x$  and  $\nu_y$ . The fraction transmitted directly from region 1 to region 2 is calculated in a similar way.

Ultimate Transmission Probability of Reflected Molecules

In performing the second stage of analysis, that of determining the ultimate probability of a molecule's getting through to region 2 after being emitted for a known position along the blades, it will be remembered that, in general, it was necessary to solve two simultaneous integral equations for  $\sigma_{x2}$  along with  $\sigma_{y2}$  which were of the form,

$$\sigma_{x2} = C_{x2} + \int \sigma_{y2} F(x,y) dy \quad (\text{Eq. A-9a})$$

and

$$\sigma_{y2} = C_{y2} + \int \sigma_{x2} F(y,x) dx \quad (\text{Eq. A-9b})$$

where  $F(x,y)dy$  was defined as the fraction of molecules emitted from  $dx$  at  $x$  which impinge directly upon the area  $dy$  at  $y$ , and  $C_{x2}$  the fraction of molecules emitted from  $dx$  at  $x$  which reach region 2 directly without any further collision with the blade surfaces.  $F(y,x)$  and  $C_{y2}$  are defined similarly.

For the case under consideration, certain simplifications are possible. First, if the cosine law of reflection is valid,  $F(x,y) = F(y,x)$ ; and second, for the case of flat plate blading, symmetry enables one to say, for equal values of  $x$  and  $y$ ,  $\sigma_{x2} = \sigma_{y1}$ , and, similarly,  $\sigma_{x1} = \sigma_{y2}$ . Furthermore, since

$$\left. \begin{aligned} \sigma_{x1} + \sigma_{x2} &= 1 \\ \sigma_{y1} + \sigma_{y2} &= 1 \end{aligned} \right\} (\text{Eq. A-10})$$

it is possible to reduce the two simultaneous equations to a single one in the form,

$$\sigma_{x2} = 1 - C_{x1} - \int \sigma_{y1} F(x,y) dy \quad (\text{Eq. A-11})$$

Since  $\tau_{x_2}(x)$  and  $\tau_{y_1}(y)$  are the same function, this equation may be solved by iterative methods once the functions for  $F(x,y)$  and  $C_{x_1}$  are known.

For the calculation of  $C_{x_1}$ , refer to Fig. A-5.

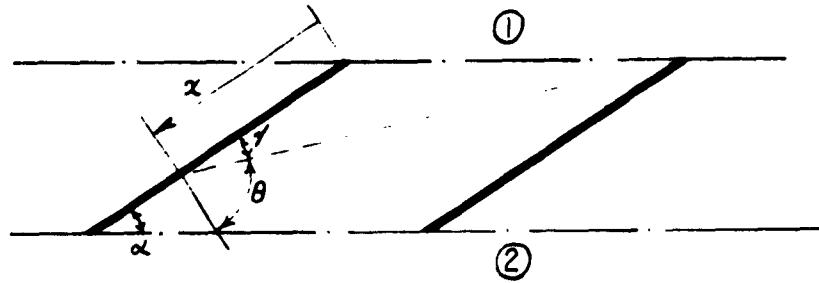


Fig. A-5

Assuming the cosine law of diffuse reflection, the fraction of molecules emitted in an angle  $d\theta$  inclined at an angle  $\theta$  to the normal is

$$\frac{1}{2} \cos \theta \, d\theta$$

Therefore the fraction emitted in the angle  $\gamma$  is

$$C_{x_1} = \frac{1}{2} \int_{\frac{\pi}{2}-\gamma}^{\pi/2} \cos \theta \, d\theta = \frac{1}{2} (1 - \cos \gamma) \quad (\text{Eq. A-12})$$

From the geometry of Fig. A-5,

$$\gamma = \cos^{-1} \left\{ \frac{\frac{s}{b} \cos \alpha + \frac{x}{b}}{\left[ \left(\frac{x}{b}\right)^2 + \left(\frac{s}{b}\right)^2 + 2 \frac{x}{b} \frac{s}{b} \cos \alpha \right]^{1/2}} \right\} \quad (\text{Eq. A-13})$$

Accordingly,

$$C_{x1} = \frac{1}{2} \left\{ 1 - \frac{\frac{s}{b} \cos \alpha + \frac{x}{b}}{\left[ \left( \frac{x}{b} \right)^2 + \left( \frac{s}{b} \right)^2 + 2 \frac{x}{b} \frac{s}{b} \cos \alpha \right]^{\frac{1}{2}}} \right\} \quad (\text{Eq. A-14})$$

For the calculation of  $F(x, y)$ , refer to Fig. A-6.

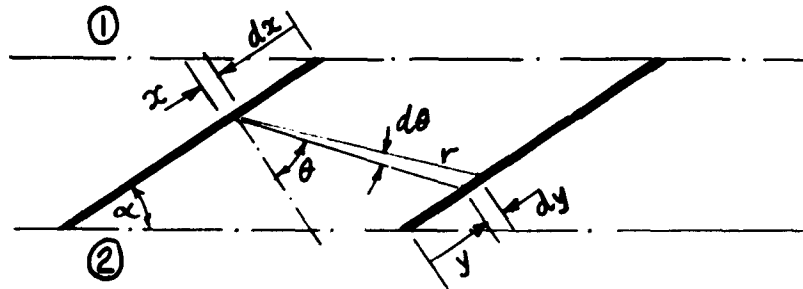


Fig. A-6

Again, by the assumption of diffuse reflection,  $F(x, y) dy$  is given by

$$F(x, y) dy = \frac{1}{2} \cos \theta d\theta$$

Referring to Fig. A-6 for the geometrical configuration,

$$\cos \theta = \frac{\frac{s}{b} \sin \alpha}{\left\{ \left( \frac{s}{b} \sin \alpha \right)^2 + \left[ \frac{y}{b} + \frac{x}{b} + \frac{s}{b} \cos \alpha - 1 \right]^2 \right\}^{1/2}} \quad (\text{Eq. A-15})$$

Also,

$$d\theta = \frac{dy \cos \theta}{r}$$

Hence

$$F(x, y) = \frac{\frac{1}{2} \left(\frac{s}{b}\right)^2 \sin^2 \alpha \, d\left(\frac{y}{b}\right)}{\left\{ \left(\frac{s}{b}\right)^2 \sin^2 \alpha + \left[ \frac{y}{b} + \frac{x}{b} + \frac{s}{b} \cos \alpha - 1 \right]^2 \right\}^{3/2}} \quad (\text{Eq. A-16})$$

APPENDIX B

DETERMINATION OF  $\Sigma_0$  IN CASCADE TESTS

As described earlier, the free-molecule cascade with zero throughflow enables one to measure directly  $\Sigma_{12}/\Sigma_0$  and  $\Sigma_{21}/\Sigma_0$  as a function of blade-speed ratio  $\dot{S}$ . Therefore, in order to obtain the magnitude of the transmission coefficients  $\Sigma_{12}$  and  $\Sigma_{21}$ , one must measure  $\Sigma_0$  for the stationary cascade. This is done by measuring pressure ratio vs. volume throughflow, and using the relationship  $n_2/n_1 = 1 - (W/\Sigma_0)$ .

In the case of the rotating-row machine, this was a straightforward task since the only appreciable resistance to flow between the upstream and downstream pressure gauges was the blade row itself. In the case of the stationary cascade, such was not the case. However, the determination of  $\Sigma_0$  was arrived at through the following considerations. Fig. B-1 is a diagram of the stationary cascade, showing the several resistances to flow between the two pressure gauges.

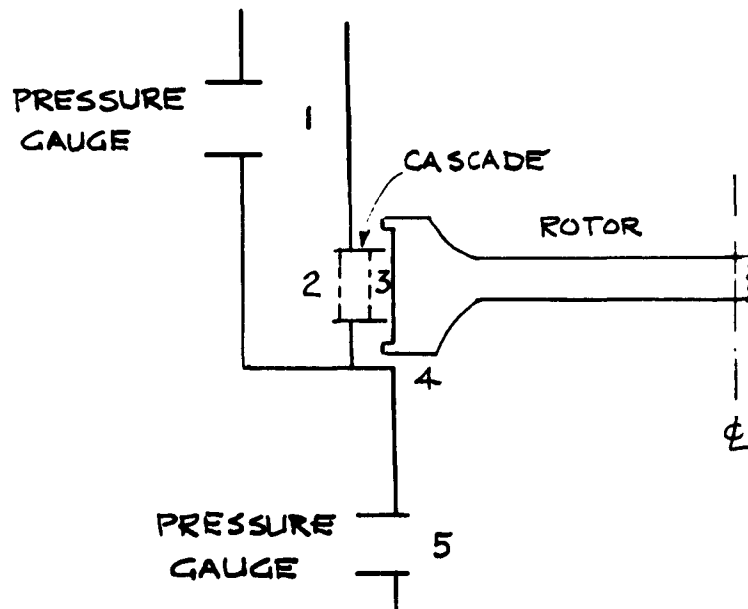


Fig. B-1

In general, if one has several flow resistances in series between two points, it is possible, from a measurement of the flow at a given pressure ratio between the two points, to determine the value of any individual resistance if all the others are known. What is desired, in this instance, is the value of the resistance from 2 to 3 when the blades are in place. This requires a knowledge of the resistances from 1 to 2, 3 to 4, and 4 to 5. Of these, only the resistance from 3 to 4 was not known and not readily calculable. Therefore it was determined by means of a preliminary experiment.

The general equation for the flow from a region  $i$  to a region  $j$  may be written as

$$\dot{N}_i A_i \Sigma_{ij} - \dot{N}_j A_j \Sigma_{ji} = W_i \dot{N}_i A_i \quad (\text{B-1})$$

where  $\dot{N}$  signifies molecular flux;  $\Sigma_{ij}$  the transmission coefficient from  $i$  to  $j$ ; and  $W_i$  the net throughflux ratio based on the incident flux  $\dot{N}_i A_i$  for region  $i$ .

In the absence of moving parts, it is further required that

$$A_i \Sigma_{ij} = A_j \Sigma_{ji} \quad (\text{B-2})$$

Applying these equations to the successive stations of Fig. B-1, we get

$$n_2/n_1 = 1 - W_1/\Sigma_{12} \quad (\text{B-3a})$$

$$n_3/n_2 = 1 - W_2/\Sigma_{23} \quad (\text{B-3b})$$

$$n_4/n_3 = 1 - W_3/\Sigma_{34} \quad (\text{B-3c})$$

$$n_5/n_4 = 1 - W_4/\Sigma_{45} \quad (\text{B-3d})$$

Since the mass flow is constant along the flow path,

$$W_i n_i A_i = K \quad (B-4)$$

where K is a constant. Now, since the positive displacement flow meter, together with the pressure gauge at 1, yields the value  $W_1$ , it is convenient to eliminate K by writing

$$W_i = W_1 \frac{n_1}{n_i} \frac{A_1}{A_i} \quad (B-5)$$

Since  $A_4/A_1 \gg 1$ , we may approximately set  $W_4 \cong 0$ . Also, since  $\Sigma_{45} \cong 1$ , it follows that  $n_5/n_4 \cong 1$

By approximating the flow between stations 1 & 2 and between 2 & 3 as flow between parallel plates, the values  $\Sigma_{12} \cong 0.33$  and  $\Sigma_{23} \cong 0.60$  are obtainable from the literature <sup>(7)</sup>. Since these passages represent relatively small resistances to the flow as compared to the passage from 3 to 4, small inaccuracies in these transmission coefficients have a very slight effect on the determination of the resistance from 3 to 4.

With these quantities known, a measurement of  $W_1$  at any given value of  $n_5/n_1$  is sufficient to solve for  $\Sigma_{34}$  using the following combination of Equations B-3 and B-5:

$$\frac{n_5}{n_1} = \left(1 - \frac{W_1}{\Sigma_{12}}\right) \left[1 - \frac{W_1}{\Sigma_{23}} \frac{A_1}{A_2} \frac{\Sigma_{12}}{\Sigma_{12} - W_1}\right] \left[1 - \frac{W_1}{\Sigma_{34}} \frac{A_1}{A_3} \left(1 - \frac{W_1}{\Sigma_{12}}\right) \left(1 - \frac{W_1}{\Sigma_{23}} \frac{A_1}{A_2} \frac{\Sigma_{12}}{\Sigma_{12} - W_1}\right)\right]$$

Numerically,  $A_1/A_2 = A_1/A_3 = 4.97$ . From Fig. 32, at  $n_5/n_1 = 0.5$ ,  $W_1 = 0.029$ . Thus one may finally calculate  $\Sigma_{34} = 0.351$ .

With this value of  $\Sigma_{34}$ , tests may be run with the blades in place, and application of the equation above to the data furnishes values of  $\Sigma_0$  (i.e.,  $\Sigma_{23}$ ) for each blade geometry.

REFERENCES

1. Becker, W., "Eine Neue Molekularpumpe", *Vakuum-Technik*, 7 Jahrgang, Heft 7, p. 149 (Oct. 1958).
2. Hablarian, M., "The Axial-Flow Compressor as a High Vacuum Pump", in Advances in Vacuum Science and Technology, Vol. I, pp. 168-172, Pergamon Press (1960).
3. Kruger, Charles H., "The Axial-Flow Compressor in the Free-Molecule Range", Ph.D. Thesis, Dept. of Mech.Eng., M.I.T., Cambridge, Mass., 1960. Also submitted as a report under Contract Nonr-1841(55) to the Office of Naval Research, Fluid Dynamics Branch.
4. Kruger, Charles H., and Shapiro, Ascher H., "Vacuum Pumping with a Bladed Axial-Flow Turbomachine", in Transactions of the Seventh National Symposium on Vacuum Technology, pp. 6-12, Pergamon Press (1961).
5. Kruger, Charles H., and Shapiro, Ascher H., "The Axial-Flow Compressor in the Free-Molecule Range", in *Rarefied Gas Dynamics*, edit. by L. Talbot, pp. 117-140, Academic Press (1961).
6. Ashley, H., "Applications of the Theory of Free Molecule Flow to Aeronautics", *Jour. Aero. Sci.*, vol. 16, No. 2, p. 95 (Feb. 1949).
7. Dushman, S., "Scientific Foundations of Vacuum Technique", John Wiley & Sons, New York (1949).
8. Davis, D. H., Levenson, L. L., and Milleron, N., "Molecular Flow Through Short Ducts", in *Rarefied Gas Dynamics*, edit. by L. Talbot, pp. 99-115, Academic Press (1961).
9. Patterson, G. N., "Molecular Flow of Gases", John Wiley & Sons, New York (1956).

TABLE I

THEORETICAL VALUES OF TRANSMISSION COEFFICIENT,  $\Sigma$ 

Note: Positive values of S correspond to  $\Sigma_{12}$ ; negative values correspond to  $\Sigma_{21}$ .

(a)  $s/b=1/4$ 

S	$\alpha$				
	10°	20°	30°	45°	60°
0.00	.0619	.0855	.1516	.2494	.3298
0.10	.0681	.0962	.1682	.2701	.3477
-0.10	.0562	.0758	.1362	.2293	.3110
0.25	.0784	.1142	.1953	.3014	.3715
-0.25	.0486	.0633	.1158	.2010	.2821
0.50	.0979	.1493	.2446	.3505	.3996
-0.50	.0383	.0473	.0888	.1606	.2361
0.75	.1203	.1893	.2953	.3896	.4094
-0.75	.0306	.0364	.0697	.1300	.1973
1.00	.1448	.2323	.3427	.4134	.4018
-1.00	.0249	.0293	.0569	.1085	.1678
2.00	.2549	.3842	.4307	.3640	.2932
-2.00	.0136	.0185	.0375	.0748	.1188
3.00	.3643	.4348	.3663	.2705	.2373
-3.00	.0095	.0156	.0325	.0667	.1077
4.00	.4560	.3946	.2824	.2323	.2217
-4.00	.0074	.0143	.0302	.0631	.1030
5.00	.5210	.3252	.2344	.2185	.2153
-5.00	.0062	.0134	.0289	.0611	.1006

(b)  $s/b=1/2$ 

S	$\alpha$				
	10°	20°	30°	45°	60°
0.00	.0544	.1432	.2370	.3642	.4617
0.10	.0615	.1599	.2609	.3919	.4842
-0.10	.0481	.1281	.2148	.3374	.4378
0.25	.0735	.1876	.2993	.4327	.5143
-0.25	.0400	.1082	.1848	.2991	.4010
0.50	.0975	.2403	.3675	.4962	.5502
-0.50	.0298	.0822	.1441	.2434	.3413
0.75	.1263	.2988	.4360	.5466	.5646
-0.75	.0227	.0640	.1146	.2000	.2898
1.00	.1591	.3599	.4987	.5283	.5579
-1.00	.0181	.0517	.0943	.1685	.2495
2.00	.3120	.5637	.6172	.5354	.4376
-2.00	.0109	.0325	.0619	.1164	.1780
3.00	.4572	.6321	.5578	.4283	.3629
-3.00	.0087	.0272	.0532	.1029	.1600
4.00	.5624	.5983	.4673	.3738	.3373
-4.00	.0077	.0245	.0490	.0967	.1521
5.00	.6206	.5299	.4047	.3500	.3261
-5.00	.0070	.0230	.0466	.0931	.1476

TABLE I (continued)

THEORETICAL VALUES OF TRANSMISSION COEFFICIENT,  $\Sigma$ (c)  $s/b=1$ 

S	$\alpha$				
	10°	20°	30°	45°	60°
0.00	.1383	.2638	.3744	.5097	.6069
0.10	.1542	.2903	.4064	.5420	.6318
-0.10	.1236	.2389	.3435	.4773	.5802
0.25	.1799	.3324	.4560	.5891	.6648
-0.25	.1039	.2048	.3003	.4297	.5382
0.50	.2274	.4066	.5389	.6596	.7045
-0.50	.0773	.1574	.2382	.3569	.4676
0.75	.2785	.4820	.6167	.7143	.7227
-0.75	.0579	.1219	.1900	.2962	.4031
1.00	.3311	.5542	.6841	.7498	.7208
-1.00	.0446	.0968	.1550	.2497	.3498
2.00	.5258	.7654	.8166	.7373	.6172
-2.00	.0234	.0562	.0965	.1672	.2455
3.00	.6736	.8491	.8012	.6536	.5356
-3.00	.0178	.0455	.0814	.1462	.2188
4.00	.7766	.8580	.7499	.5980	.4994
-4.00	.0151	.0405	.0744	.1367	.2074
5.00	.8433	.8365	.7048	.5665	.4816
-5.00	.0135	.0376	.0703	.1312	.2008

(d)  $s/b=3/2$ 

S	$\alpha$				
	10°	20°	30°	45°	60°
0.00	.3615	.4236	.4927	.5913	.6761
0.10	.3785	.4501	.5234	.6218	.6989
-0.10	.3447	.3973	.4621	.5604	.6513
0.25	.4042	.4900	.5693	.6655	.7285
-0.25	.3199	.3589	.4170	.5137	.6113
0.50	.4468	.5555	.6426	.7301	.7631
-0.50	.2802	.2985	.3465	.4388	.5412
0.75	.4887	.6179	.7089	.7809	.7783
-0.75	.2431	.2445	.2842	.3715	.4734
1.00	.5292	.6752	.7656	.8158	.7758
-1.00	.2092	.1979	.2320	.3151	.4132
2.00	.6710	.8411	.8870	.8278	.6825
-2.00	.1079	.0860	.1177	.1946	.2770
3.00	.7784	.9174	.8961	.7699	.6054
-3.00	.0536	.0508	.0875	.1623	.2396
4.00	.8555	.9400	.8719	.7256	.5703
-4.00	.0285	.0417	.0789	.1509	.2261
5.00	.9080	.9387	.8472	.6983	.5545
-5.00	.0184	.0385	.0748	.1449	.2188

THEORETICAL VALUES OF TRANSMISSION COEFFICIENT,  $\Sigma$

(e)  $s/b=2$

S	$\alpha$				
	$10^\circ$	$20^\circ$	$30^\circ$	$45^\circ$	$60^\circ$
0.00	.5147	.5536	.6052	.6849	.7498
0.10	.5282	.5761	.6322	.7117	.7703
-0.10	.5012	.5310	.5778	.6569	.7273
0.25	.5484	.6094	.6717	.7494	.7970
-0.25	.4810	.4972	.5366	.6137	.6907
0.50	.5815	.6630	.7331	.8033	.8286
-0.50	.4478	.4420	.4691	.5412	.6251
0.75	.6137	.7129	.7869	.8439	.8437
-0.75	.4155	.3895	.4055	.4717	.5588
1.00	.6445	.7581	.8318	.8704	.8439
-1.00	.3843	.3408	.3478	.4087	.4967
2.00	.7520	.8864	.9245	.8749	.7712
-2.00	.2752	.1918	.1879	.2443	.3307
3.00	.8334	.9447	.9319	.8273	.7001
-3.00	.1912	.1084	.1181	.1838	.2699
4.00	.8920	.9629	.9153	.7894	.6600
-4.00	.1294	.0678	.0927	.1643	.2497
5.00	.9322	.9636	.8980	.7647	.6386
-5.00	.0858	.0502	.0837	.1563	.2408

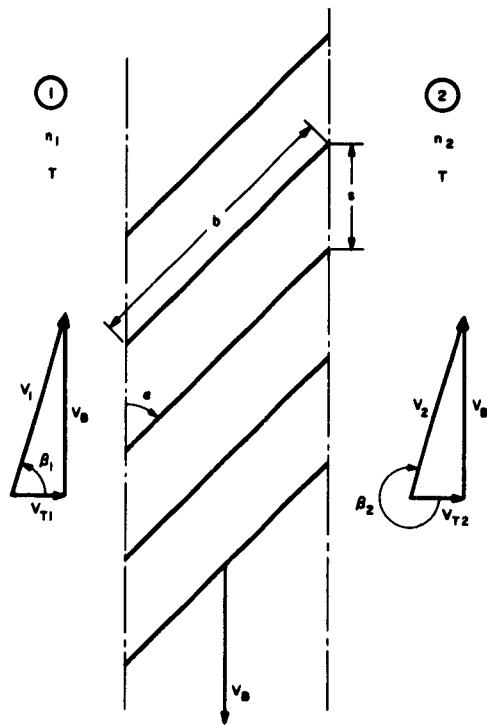


FIG. 1

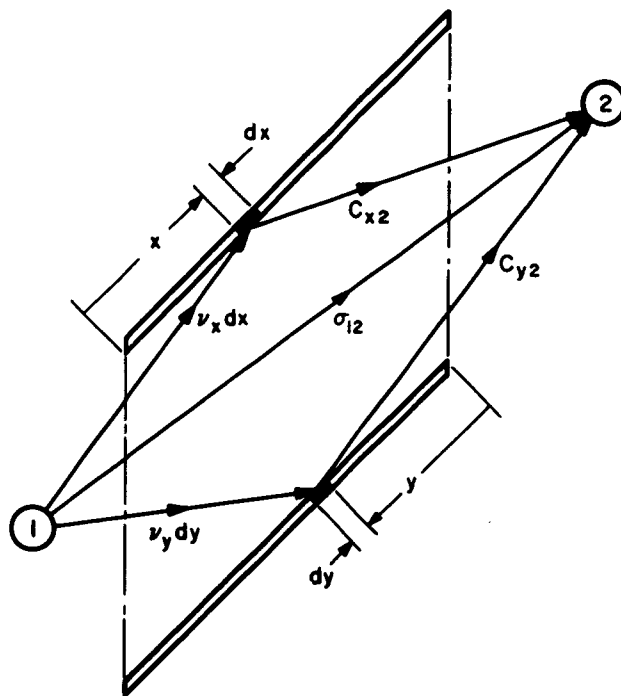


FIG. 2

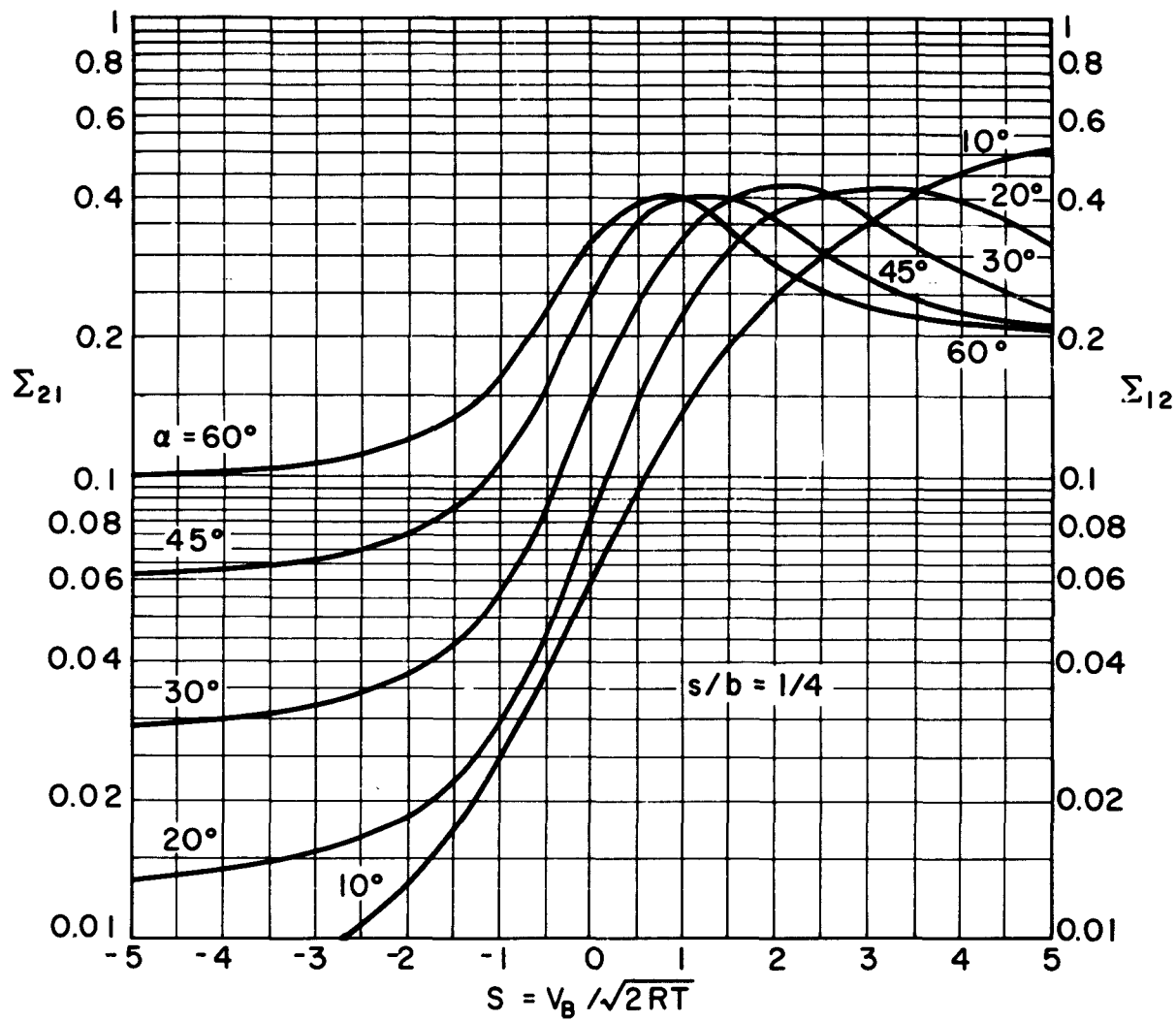


FIG. 3  
 THEORETICAL TRANSMISSION COEFFICIENTS FOR SINGLE  
 ROW,  $s/b = 1/4$

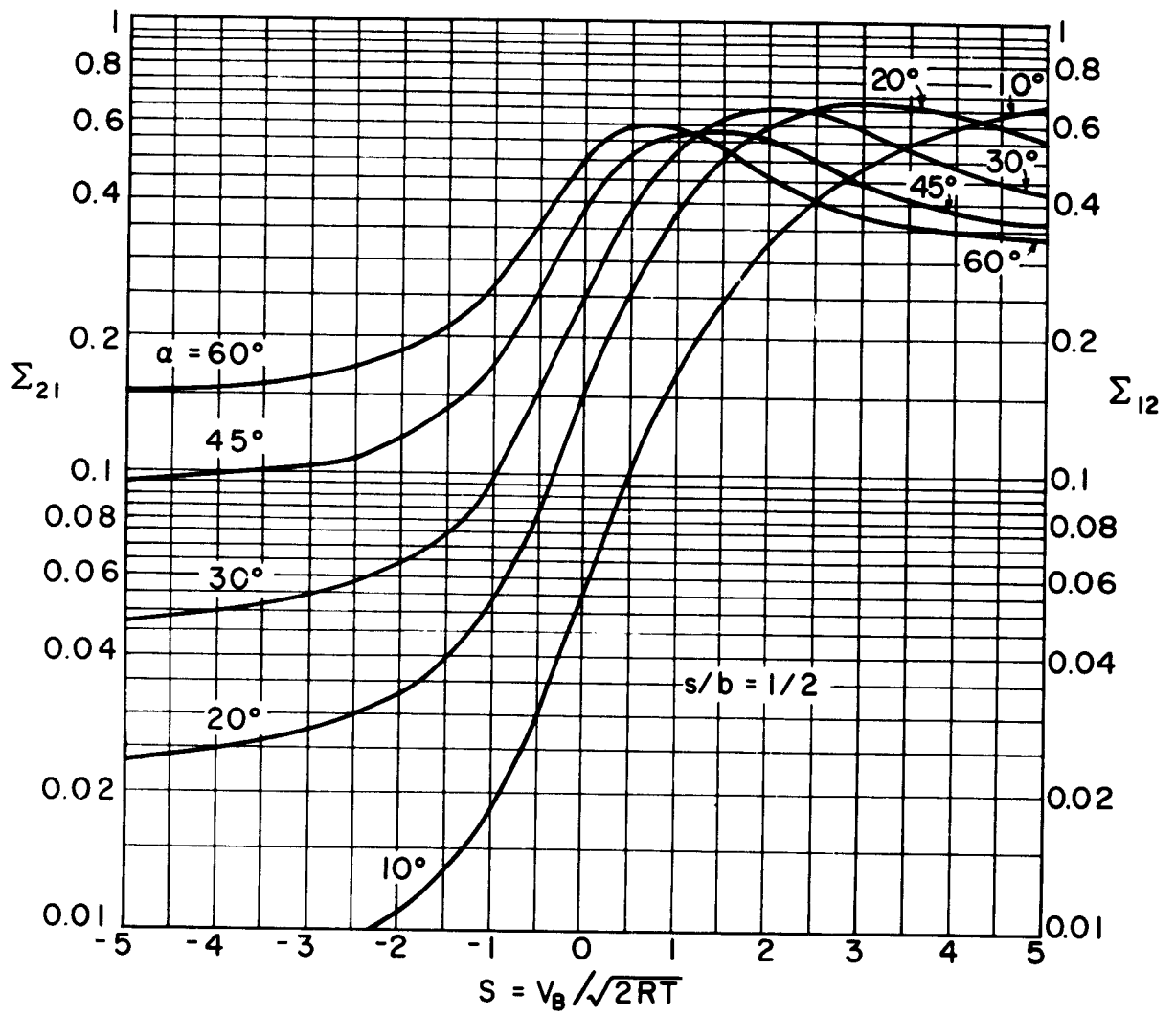


FIG. 4  
 THEORETICAL TRANSMISSION COEFFICIENTS FOR SINGLE  
 ROW,  $s/b = 1/2$

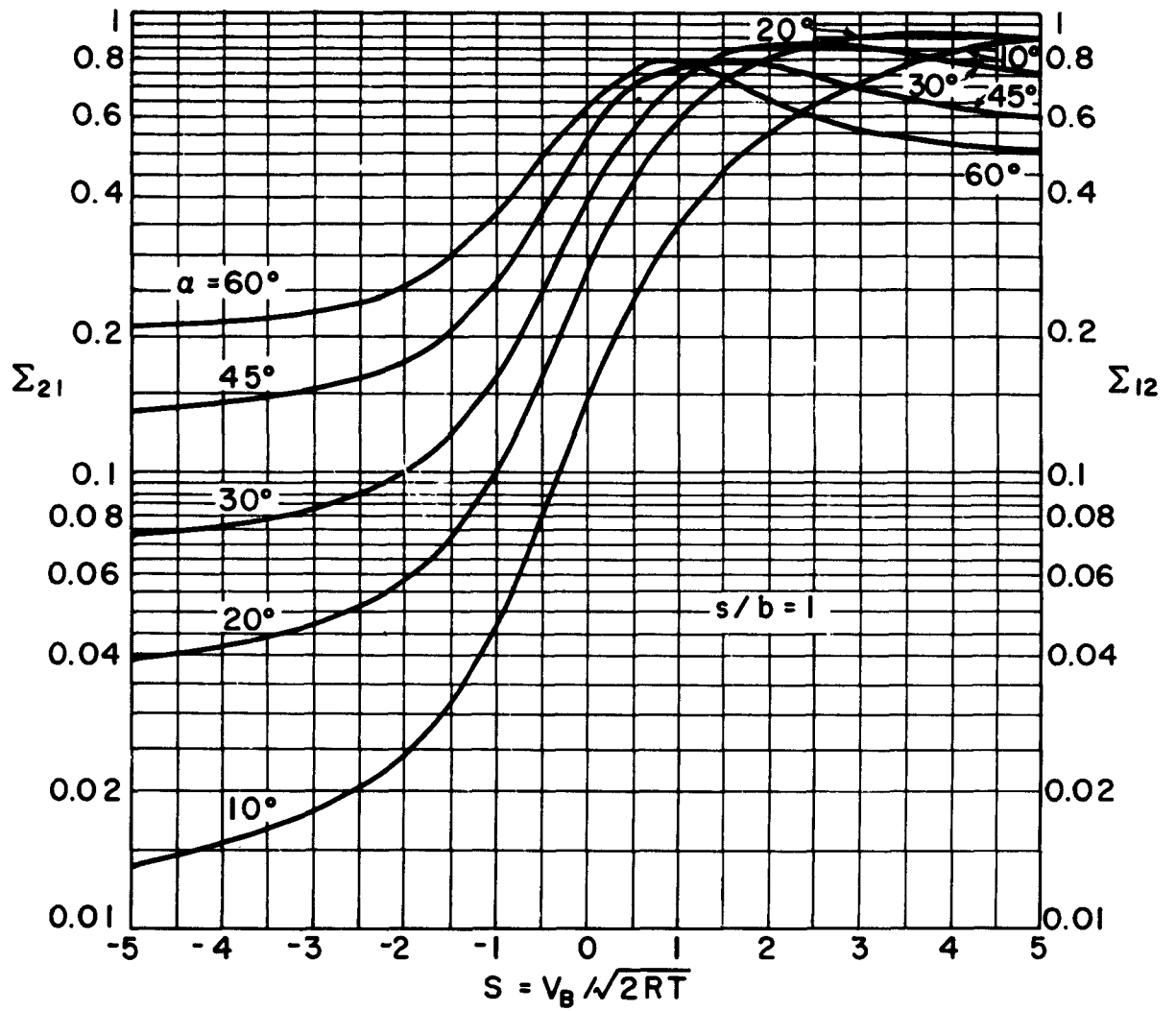


FIG. 5  
 THEORETICAL TRANSMISSION COEFFICIENTS FOR SINGLE  
 ROW,  $s/b = 1$

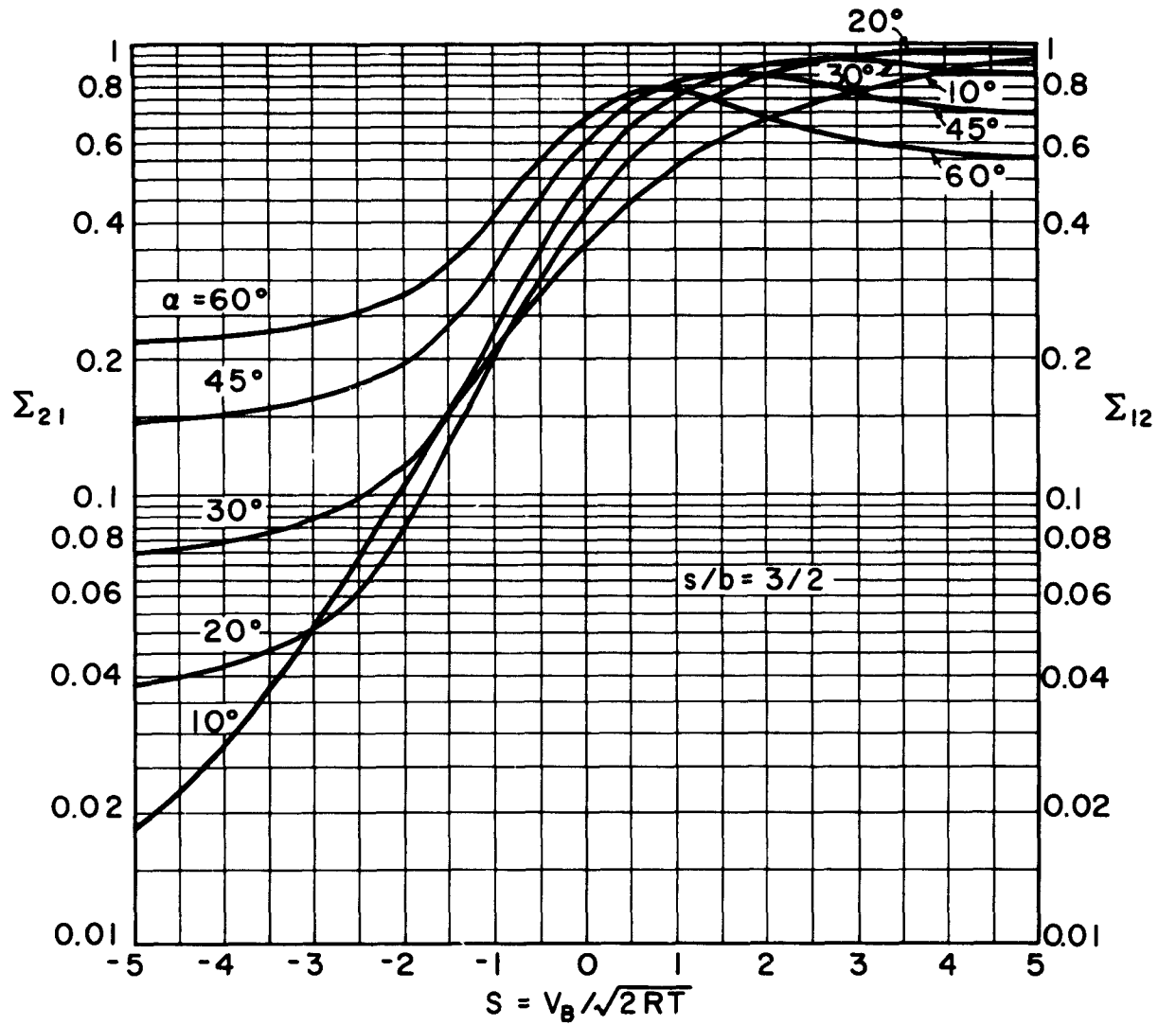


FIG. 6  
 THEORETICAL TRANSMISSION COEFFICIENTS FOR SINGLE  
 ROW,  $s/b = 3/2$

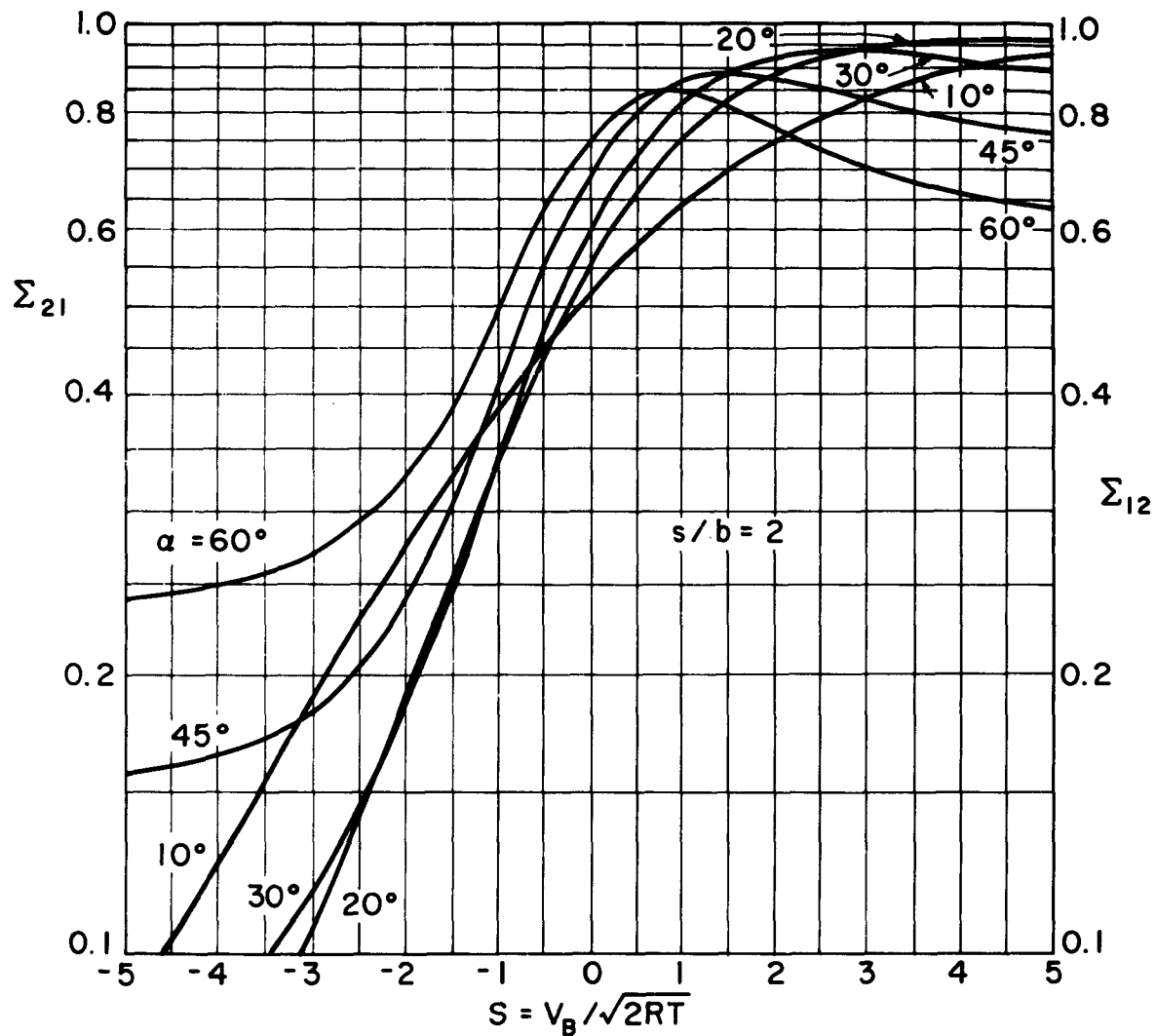


FIG. 7

THEORETICAL TRANSMISSION COEFFICIENTS FOR SINGLE ROW,  $s/b = 2$

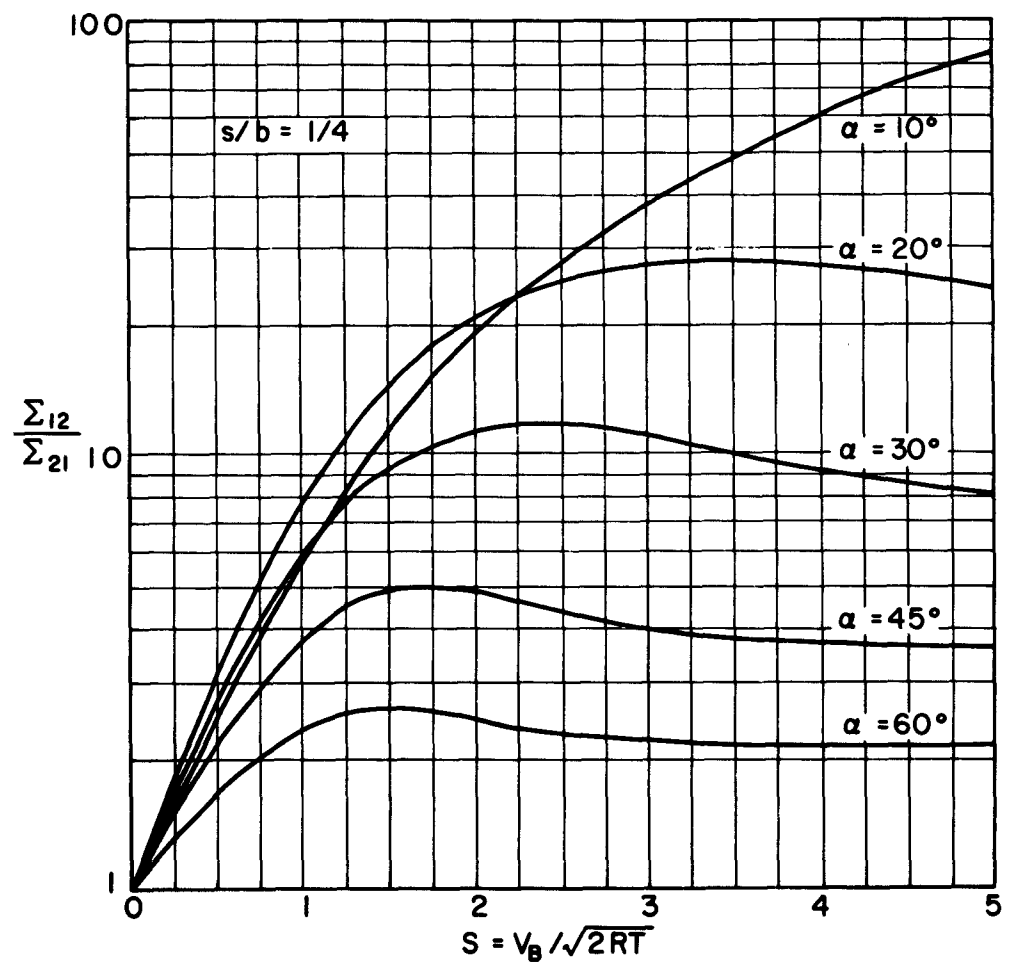
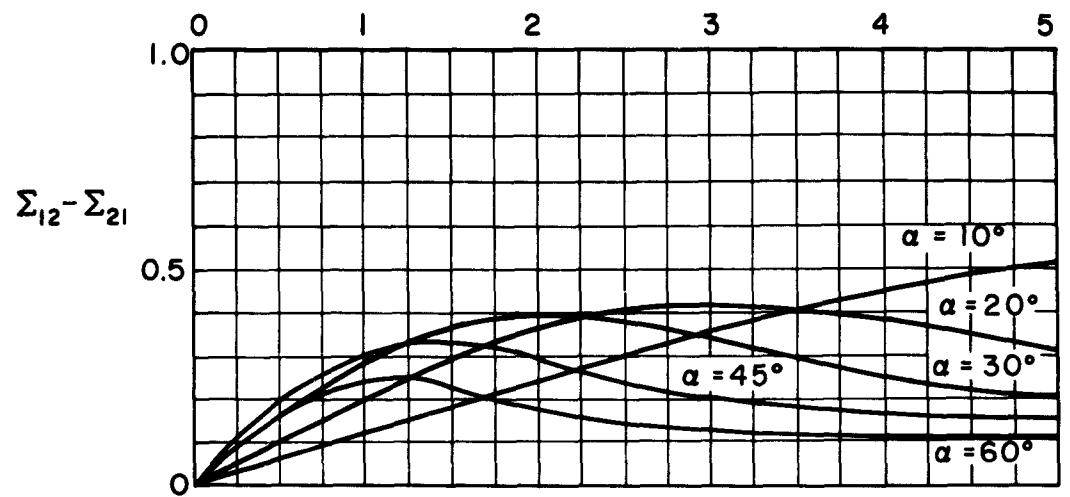


FIG. 8  
 THEORETICAL VALUES OF  $W$  FOR ZERO PRESSURE RISE ( $\Sigma_{12} - \Sigma_{21}$ ), AND OF  $n_2/n_1$  FOR ZERO FLOW ( $\Sigma_{12} / \Sigma_{21}$ ), FOR  $s/b = 1/4$

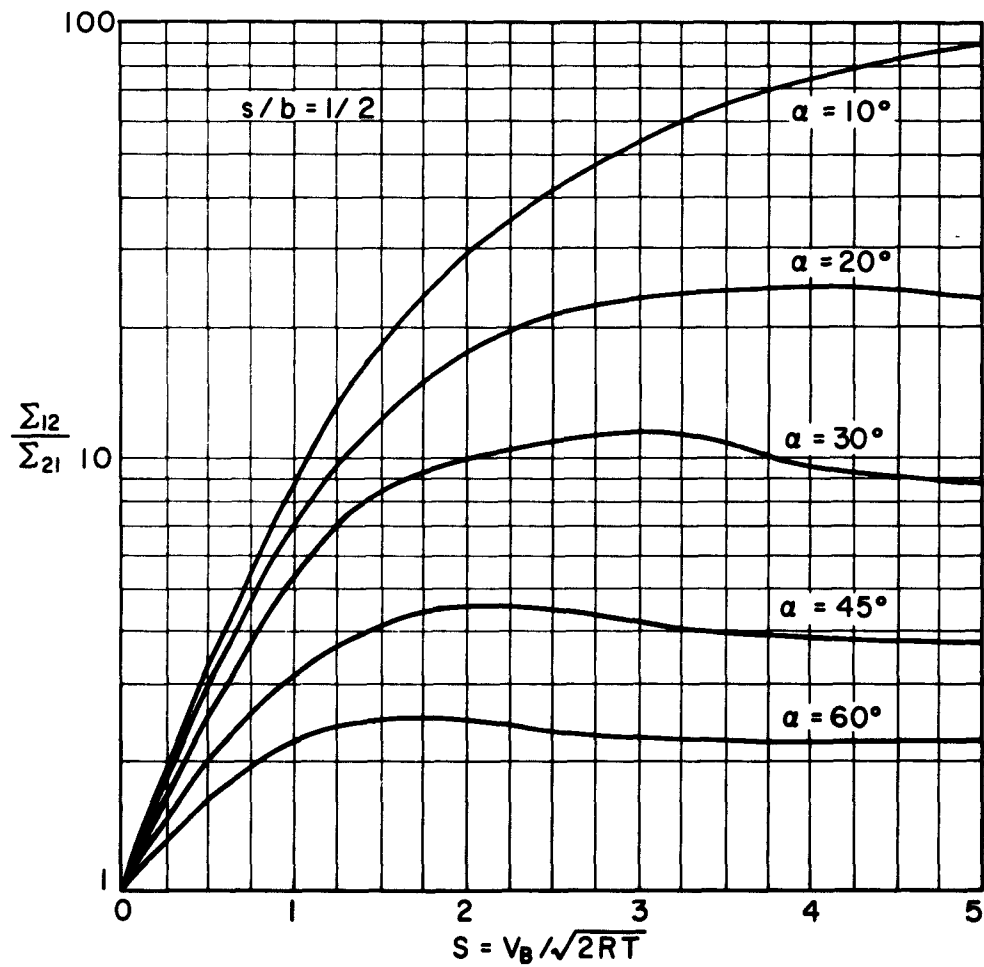
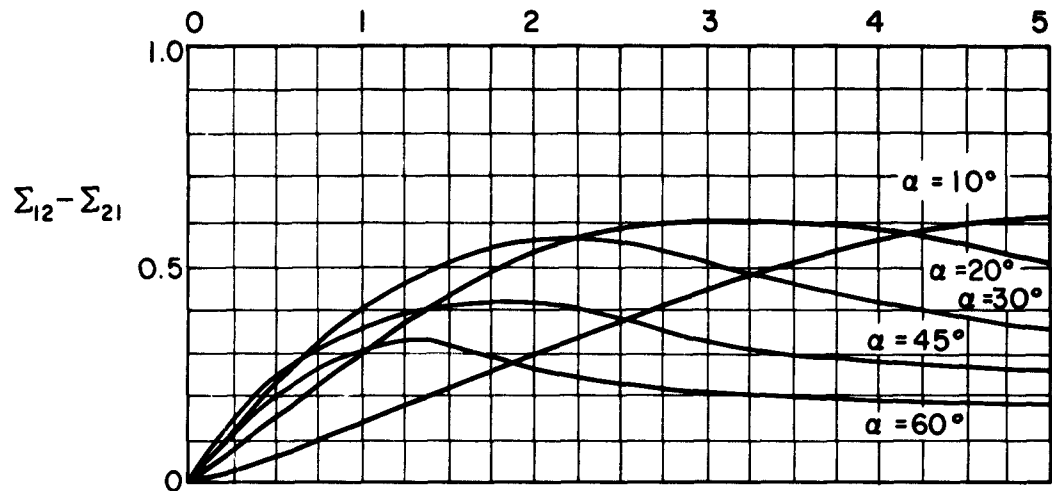


FIG. 9

THEORETICAL VALUES OF  $W$  FOR ZERO PRESSURE RISE ( $\Sigma_{12} - \Sigma_{21}$ ), AND OF  $n_2/n_1$  FOR ZERO FLOW ( $\Sigma_{12} / \Sigma_{21}$ ), FOR  $s/b = 1/2$

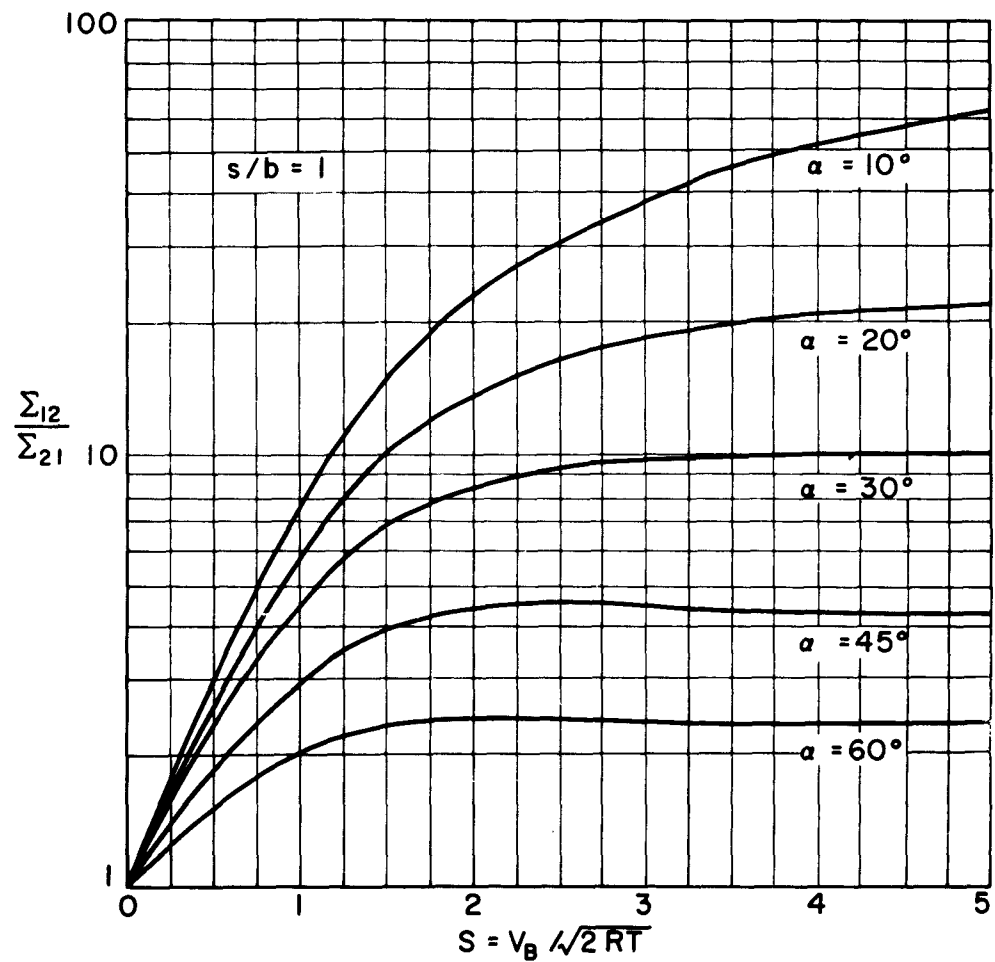
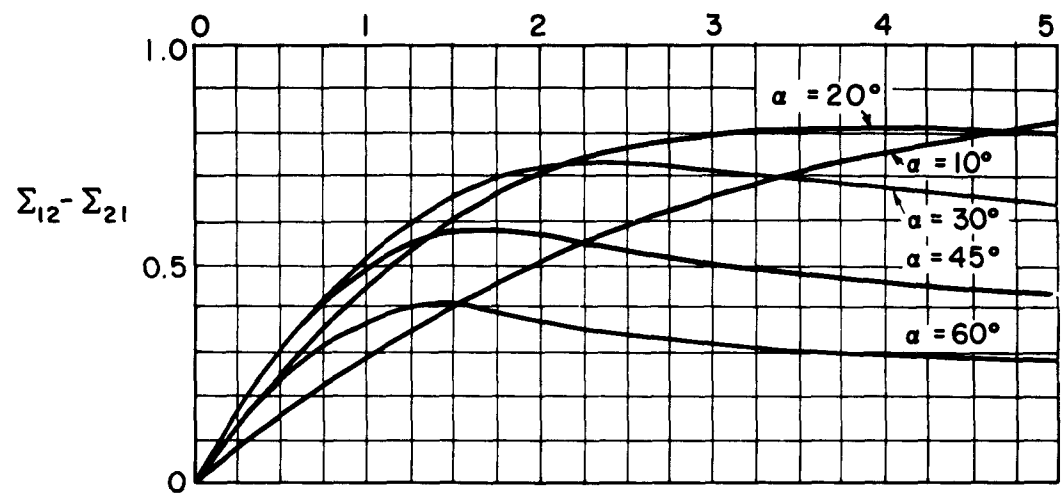


FIG. 10

THEORETICAL VALUES OF  $w$  FOR ZERO PRESSURE RISE ( $\Sigma_{12} - \Sigma_{21}$ ), AND OF  $n_2/n_1$  FOR ZERO FLOW ( $\Sigma_{12}/\Sigma_{21}$ ), FOR  $s/b = 1$

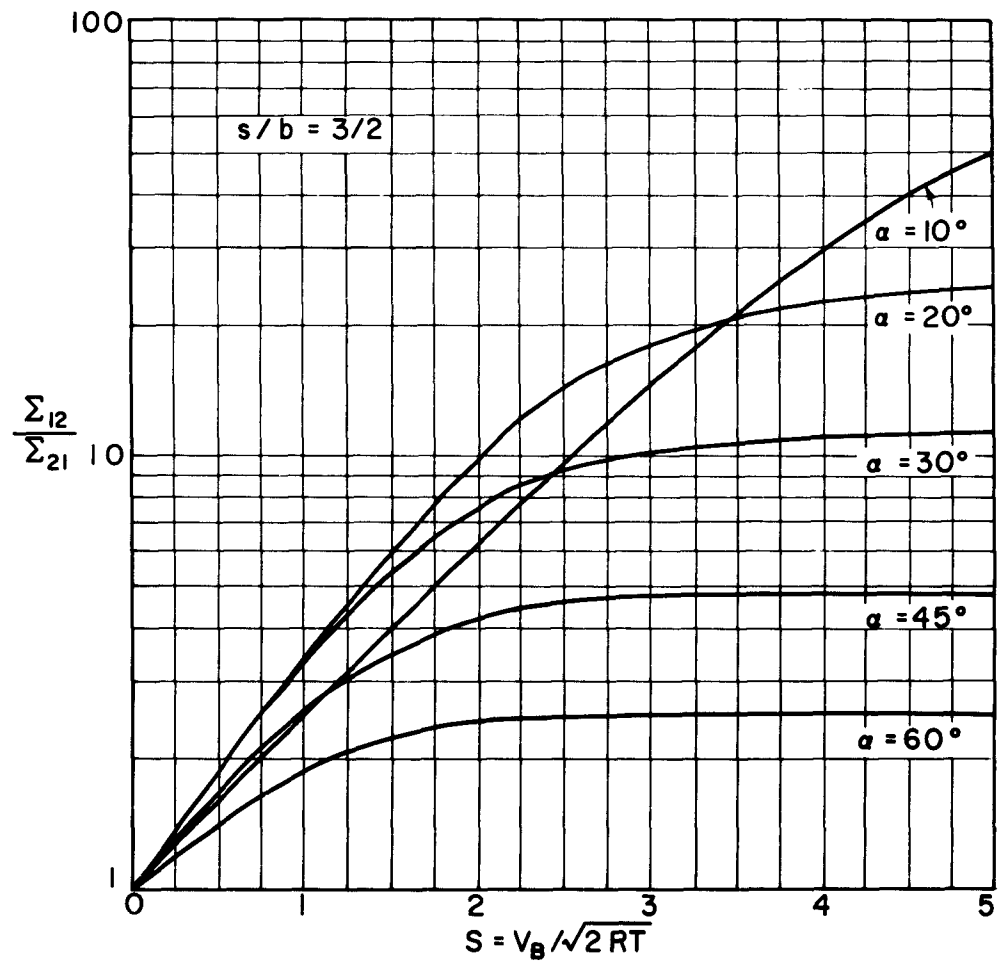
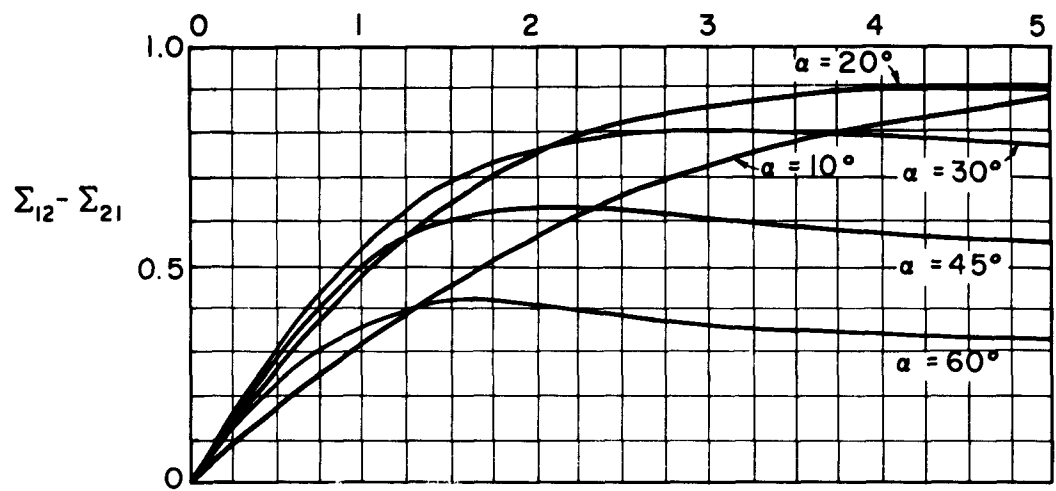


FIG. 11

THEORETICAL VALUES OF  $W$  FOR ZERO PRESSURE RISE ( $\Sigma_{12} - \Sigma_{21}$ ), AND OF  $n_2/n_1$  FOR ZERO FLOW ( $\Sigma_{12}/\Sigma_{21}$ ), FOR  $s/b = 3/2$

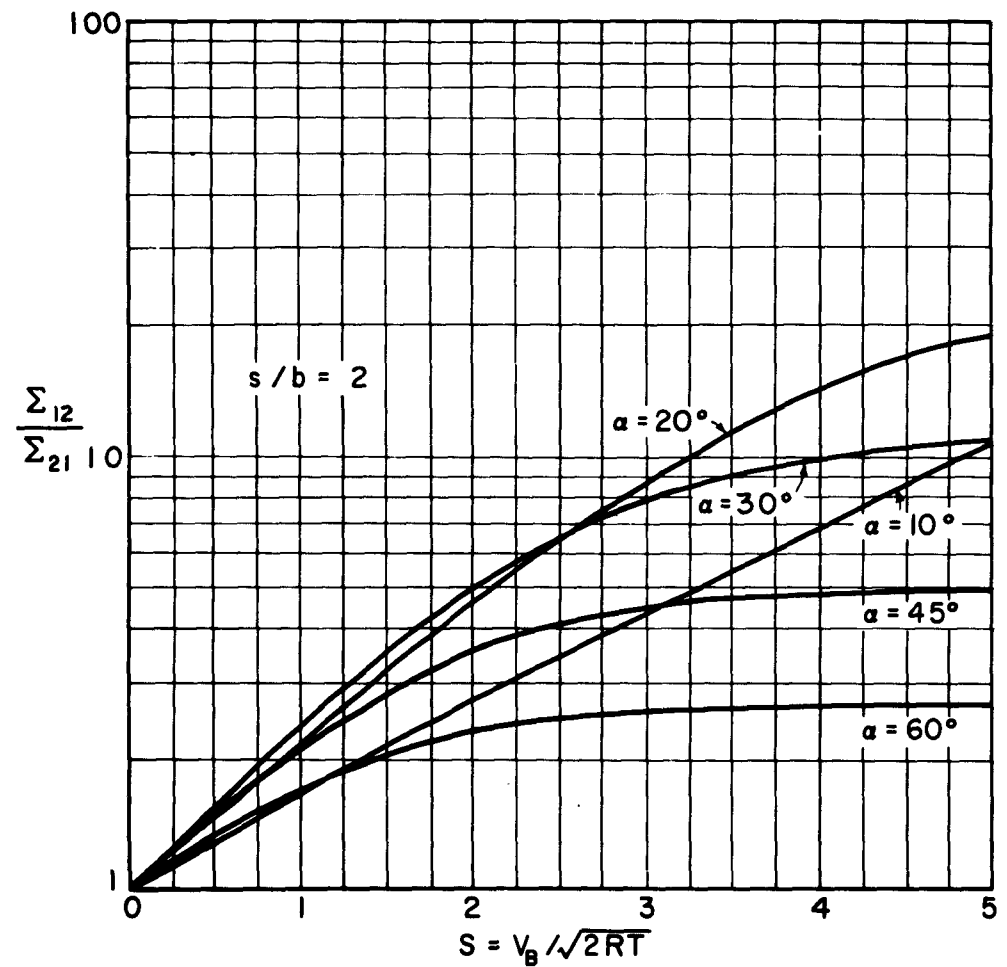
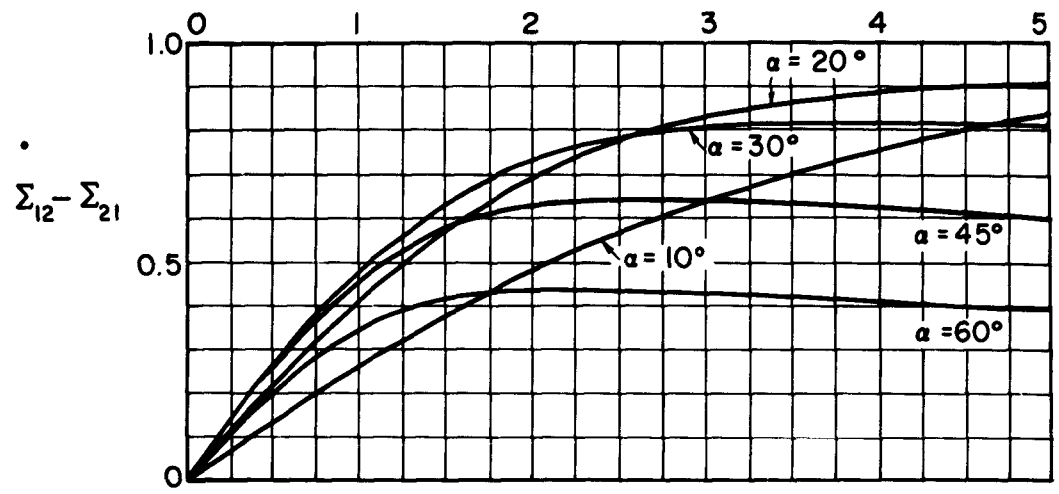


FIG. 12  
 THEORETICAL VALUES OF  $W$  FOR ZERO PRESSURE RISE ( $\Sigma_{12} - \Sigma_{21}$ ), AND OF  $n_2/n_1$  FOR ZERO FLOW ( $\Sigma_{12} / \Sigma_{21}$ ), FOR  $s/b = 2$

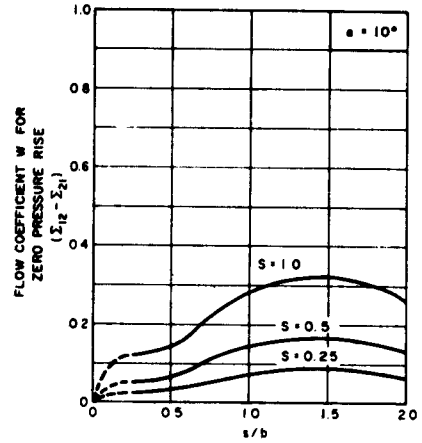
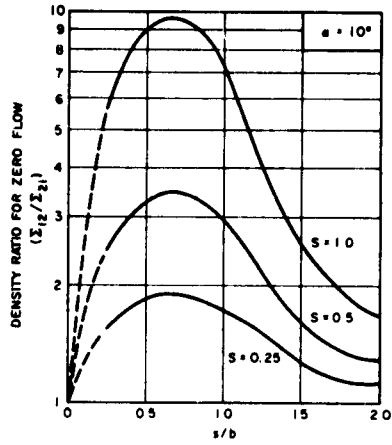


FIG 13

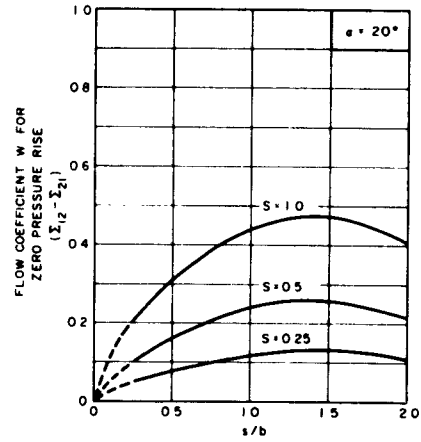
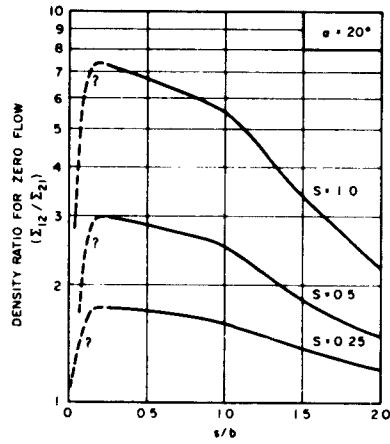


FIG 14

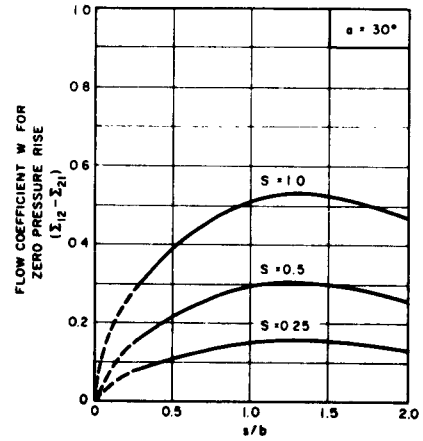
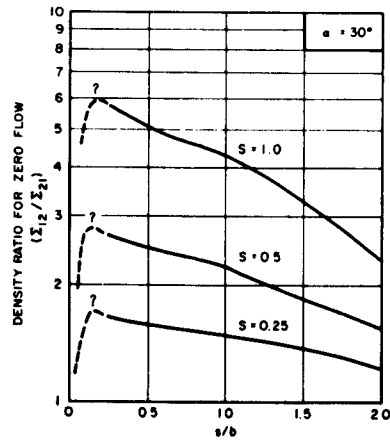


FIG 15

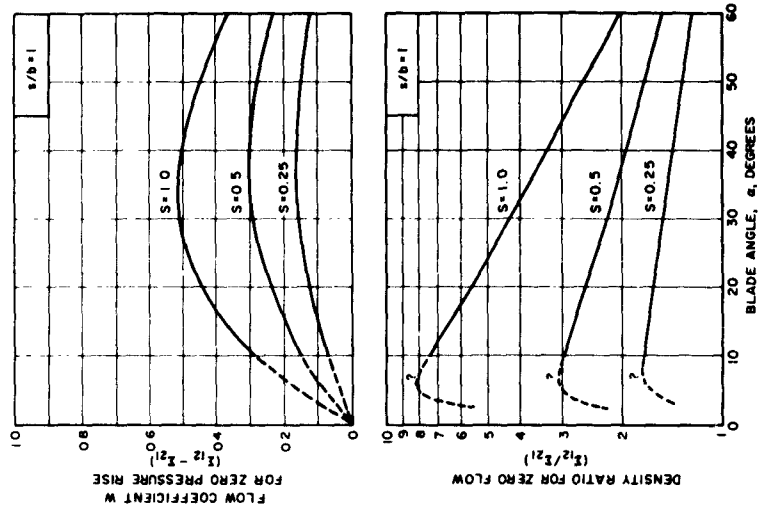


FIG. 16

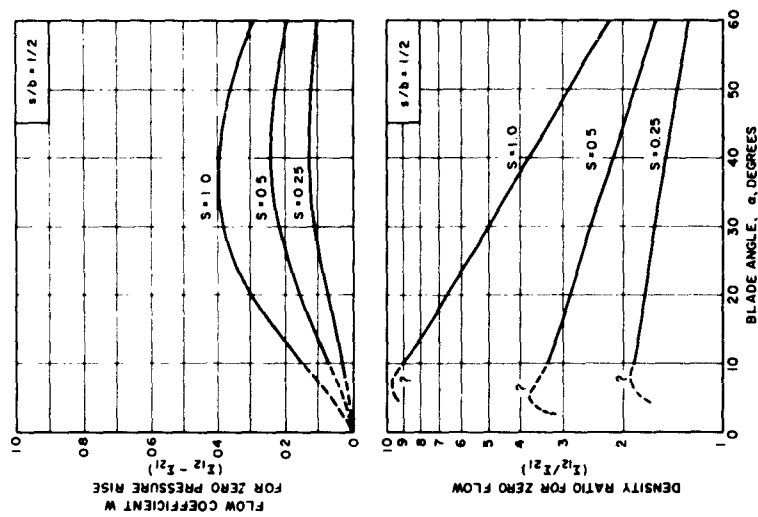


FIG. 17

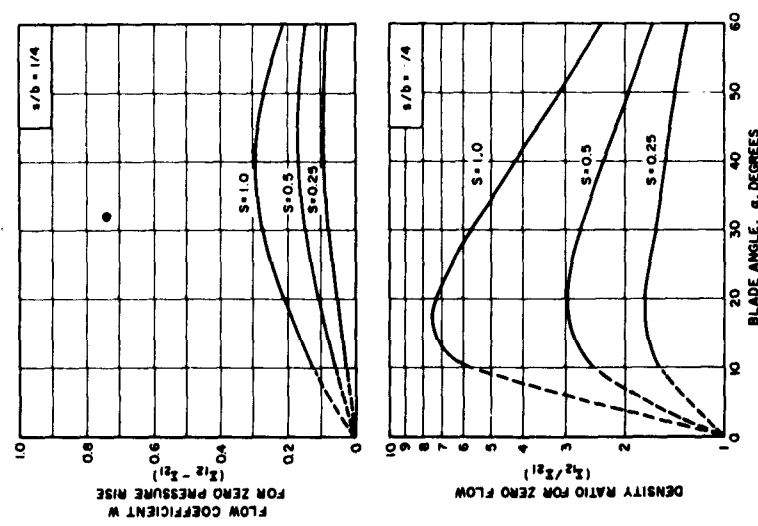


FIG. 18

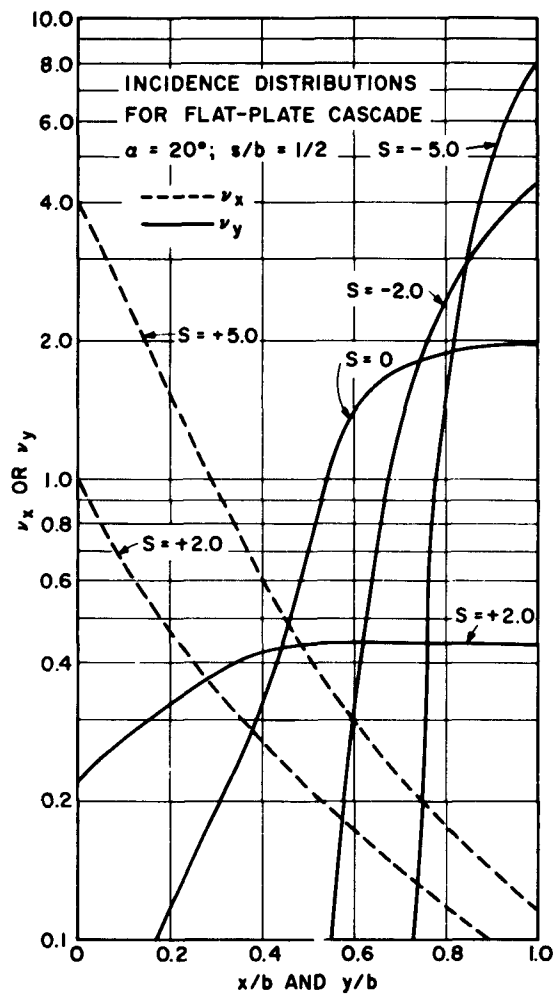


FIGURE 19

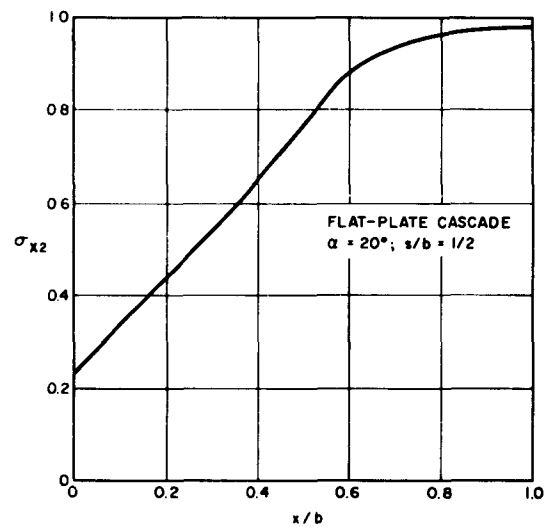


FIG. 20

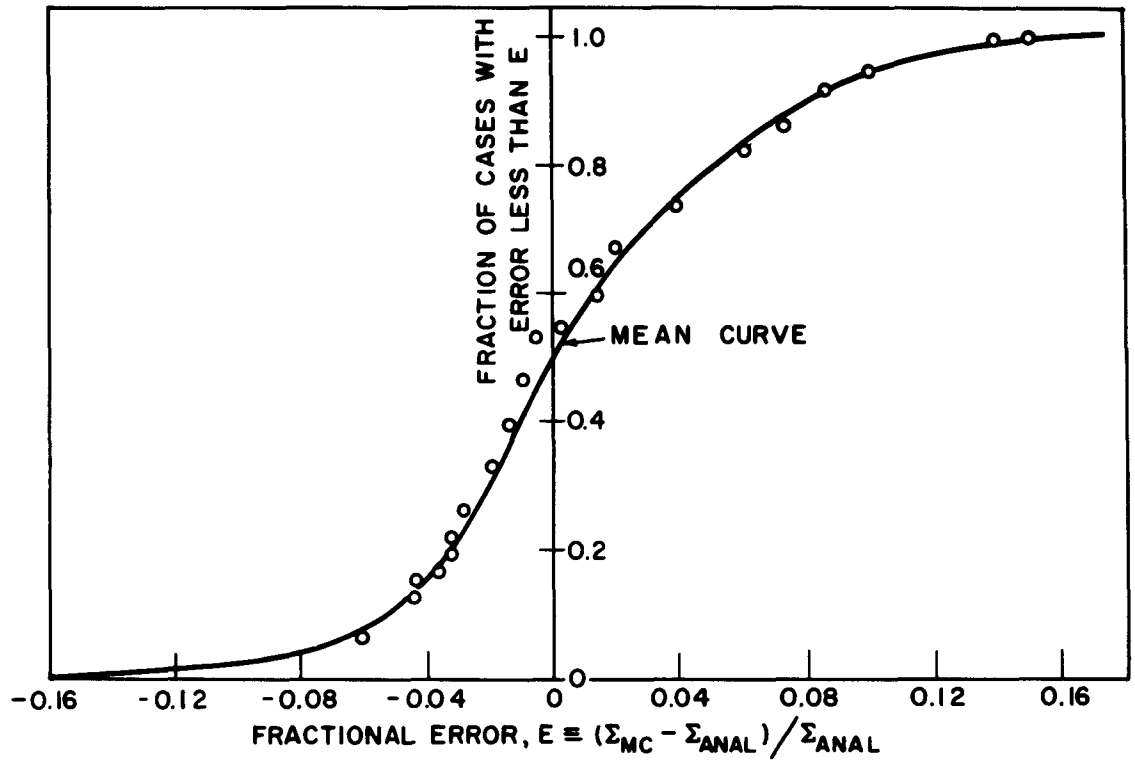


FIG. 21a

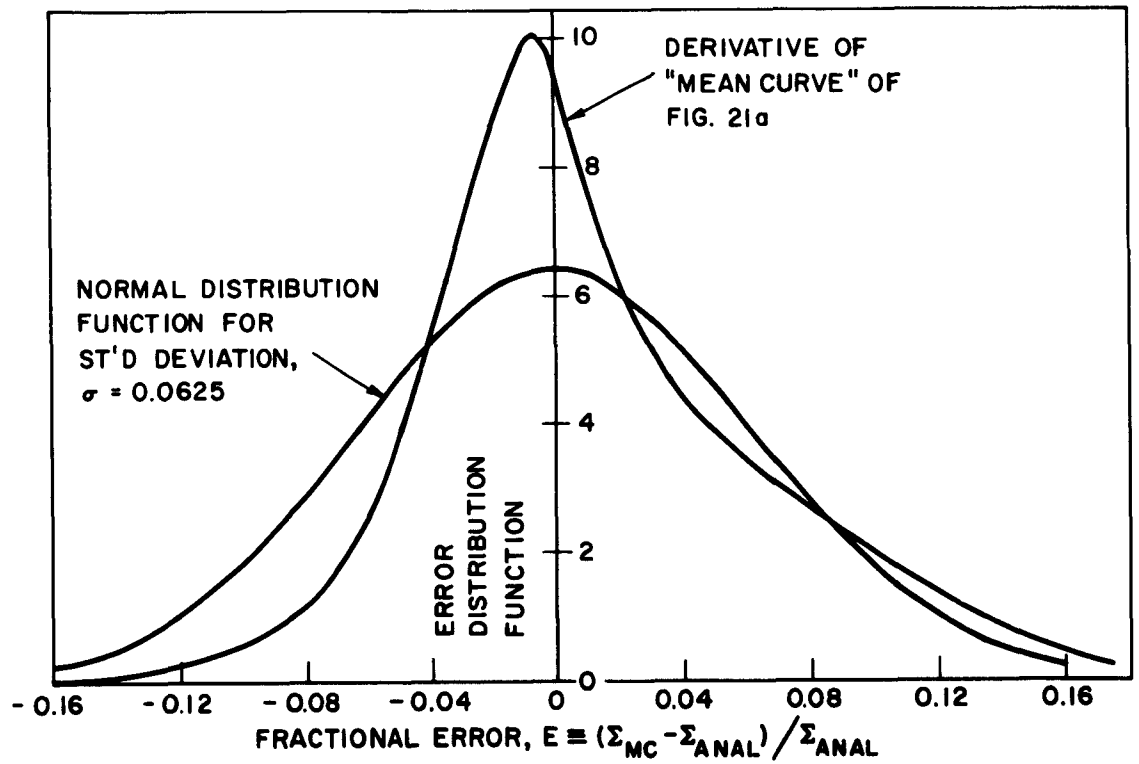


FIG. 21b

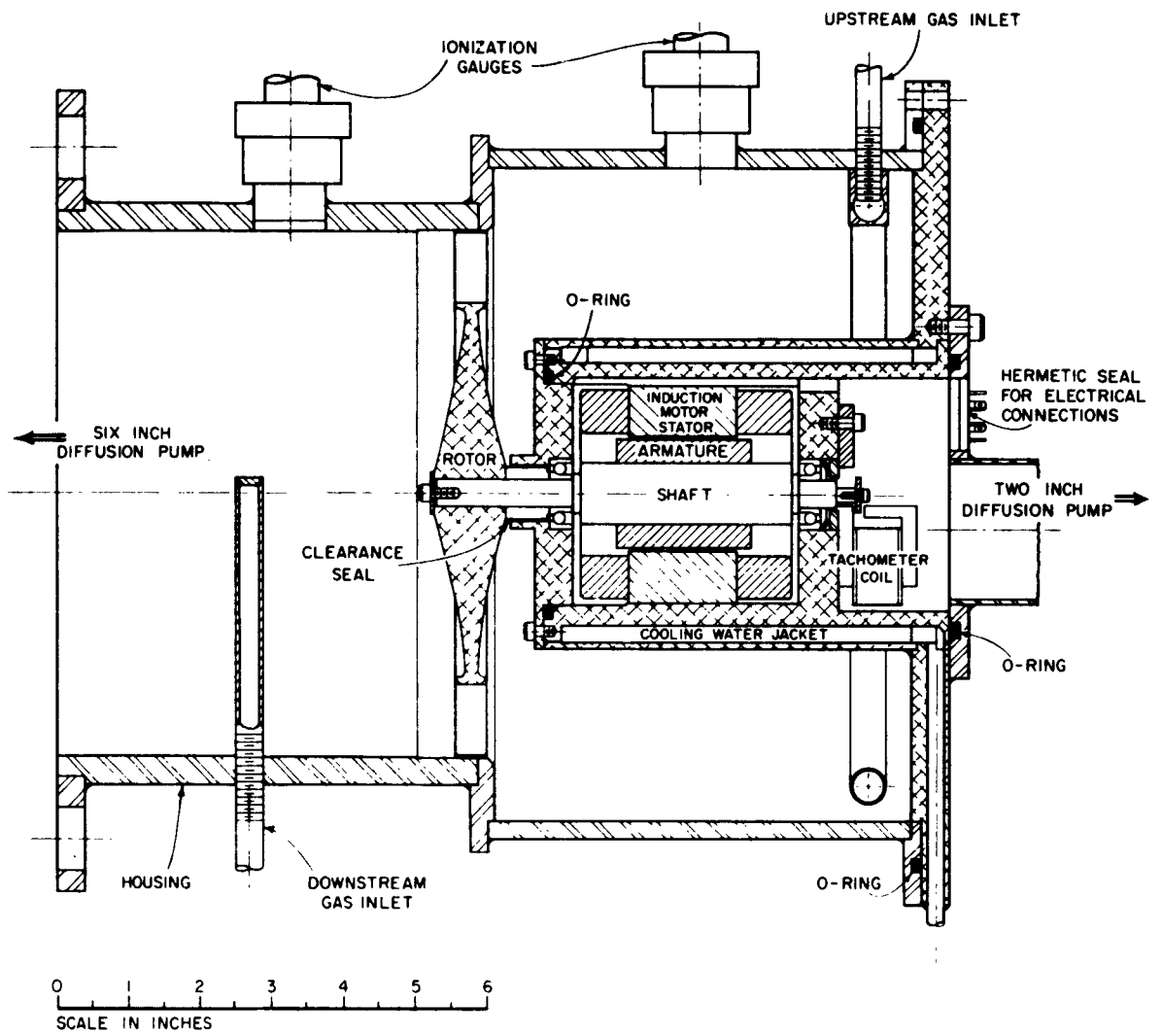


FIG. 22

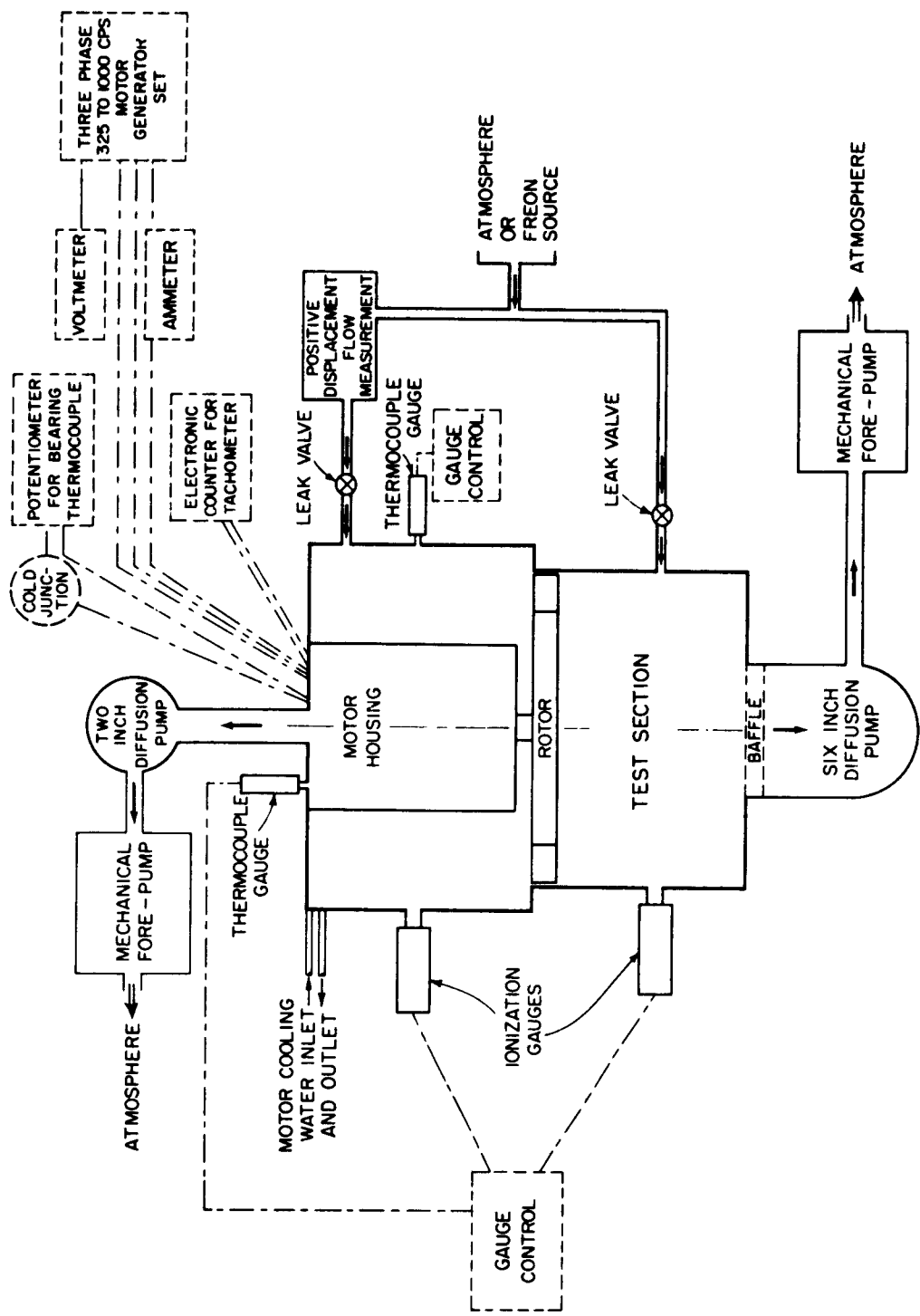


FIG 23

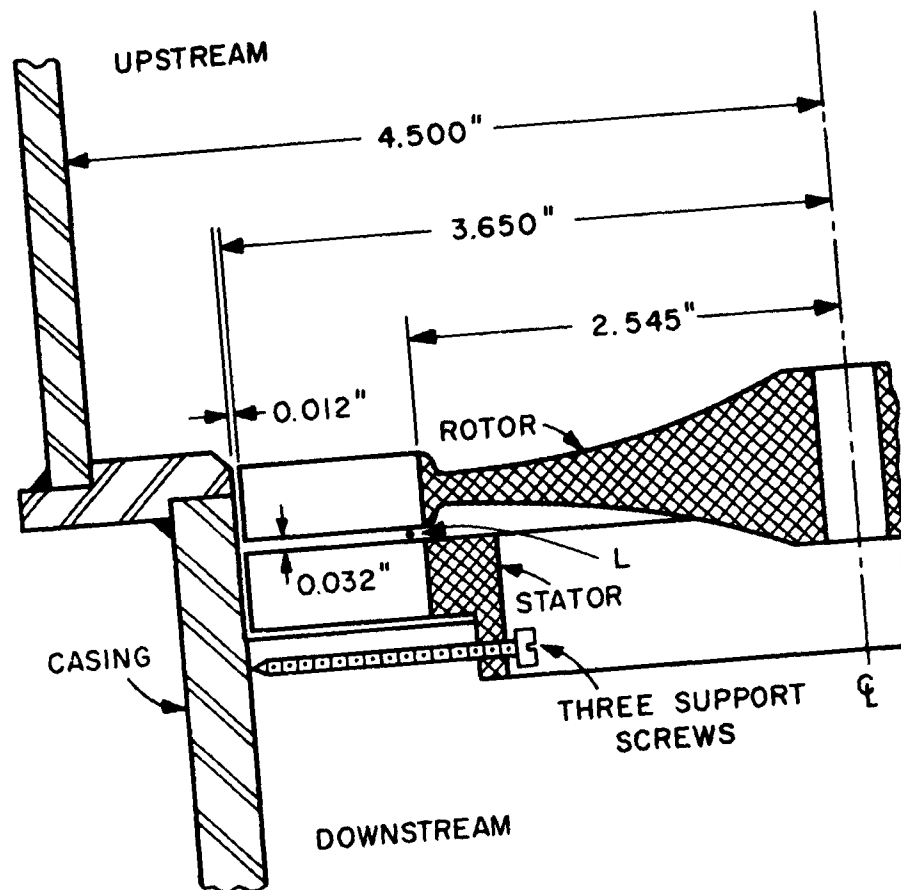


FIG. 24

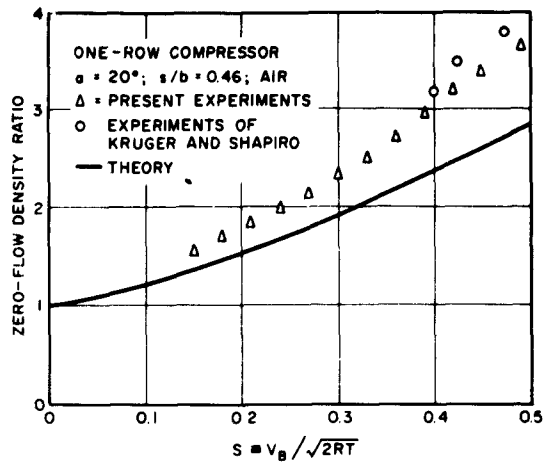


FIG 25

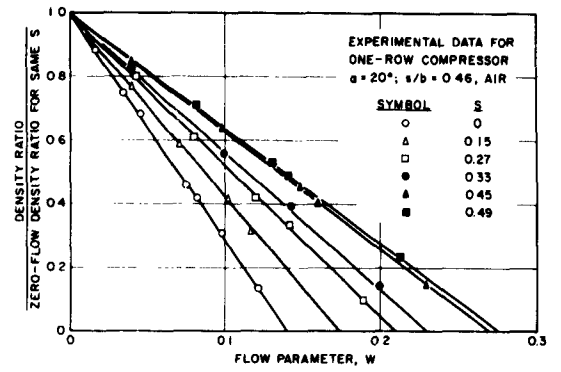


FIG 26

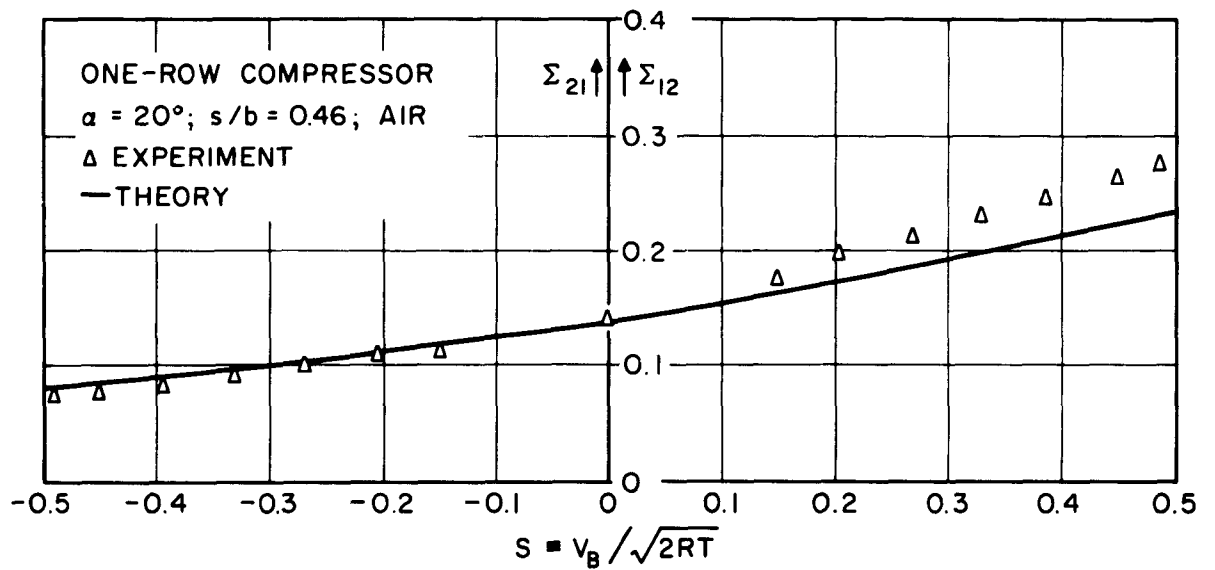


FIG. 27

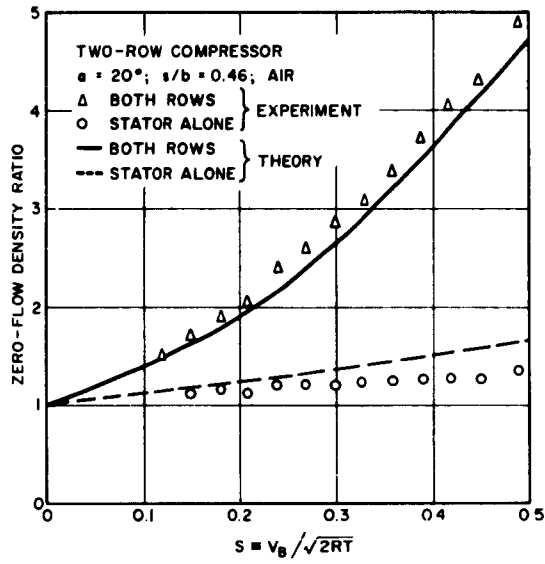


FIG 28

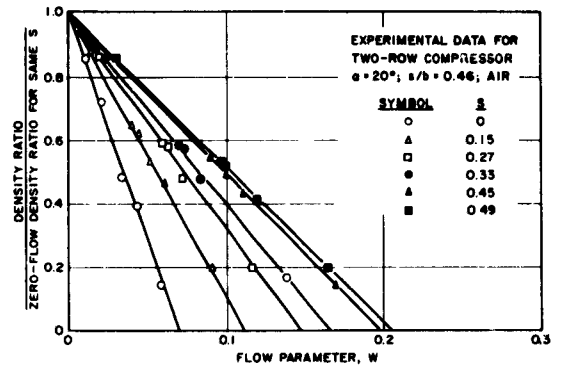


FIG 29

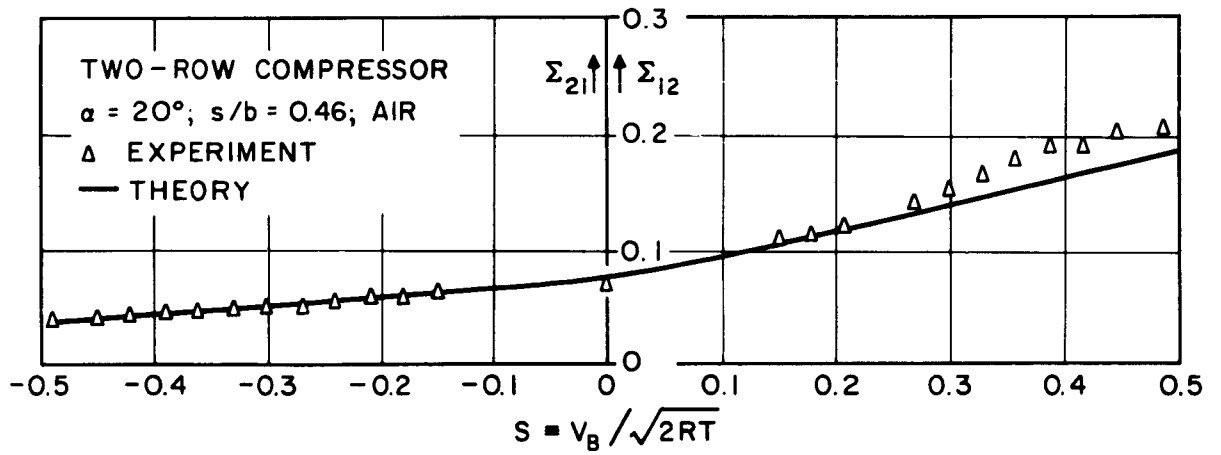


FIG 30

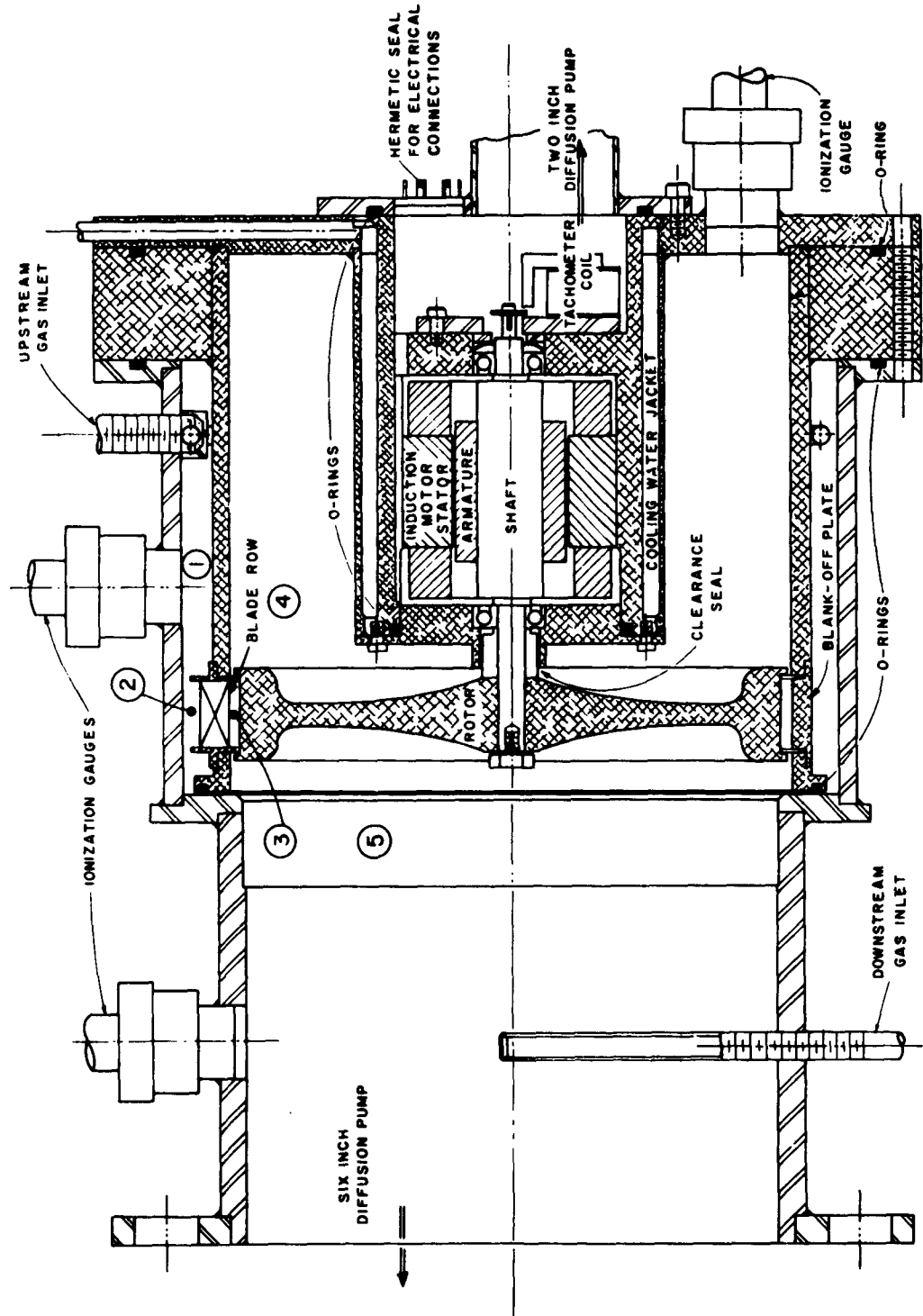
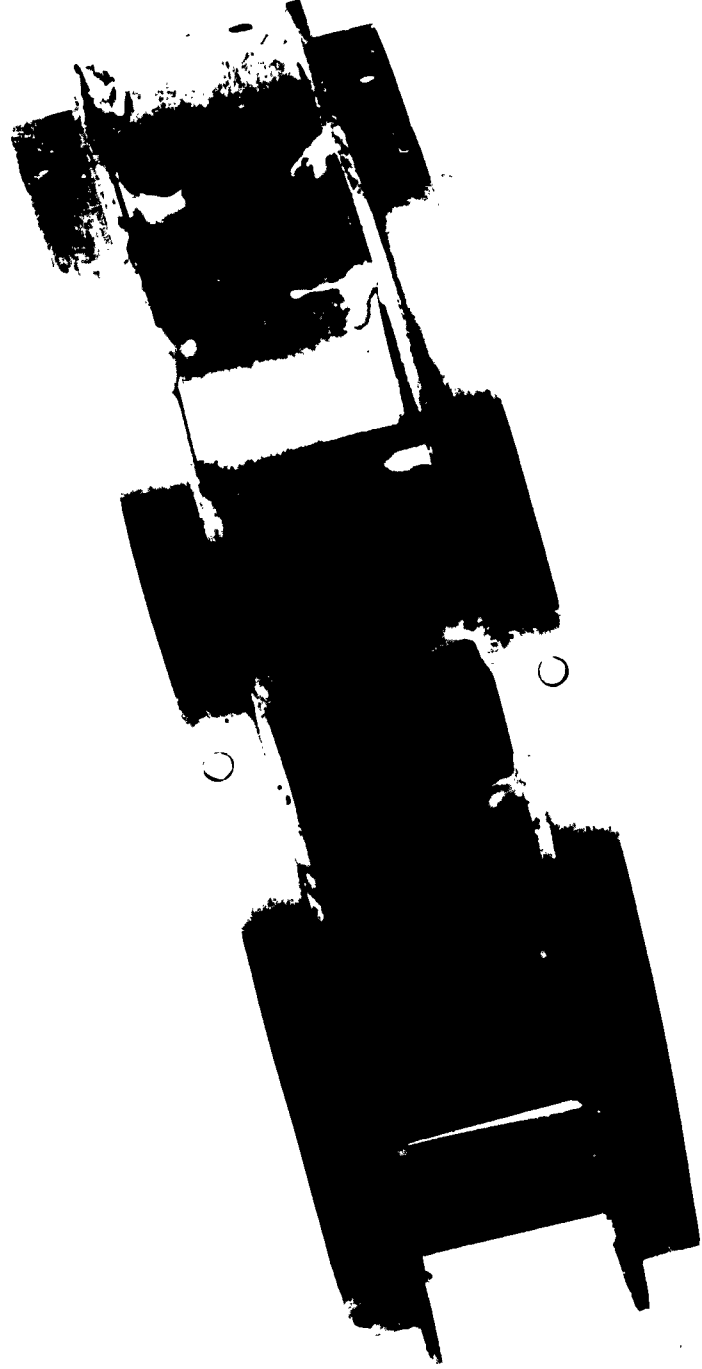


FIG. 31a



STATIONARY CASCADE RING

FIG. 31b

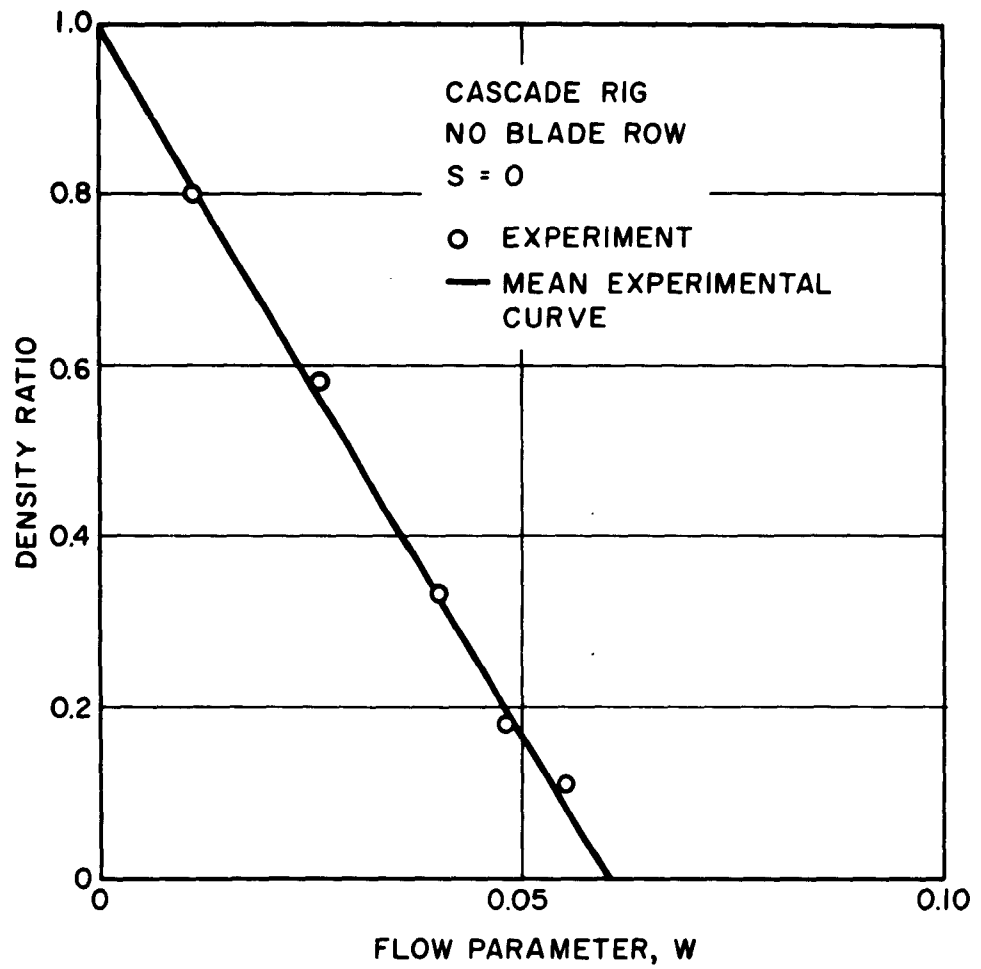


FIG. 32

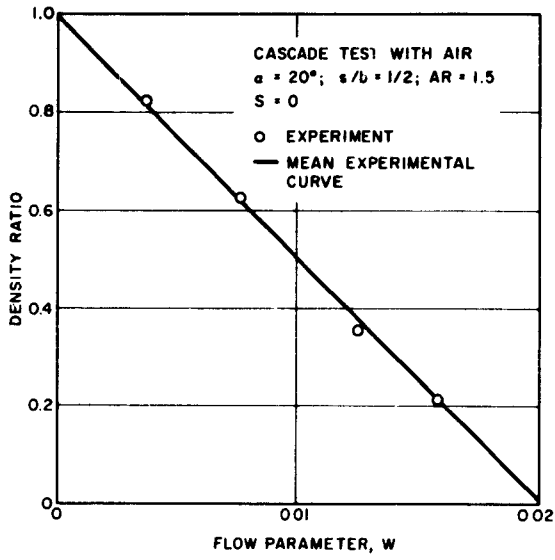


FIG. 33a

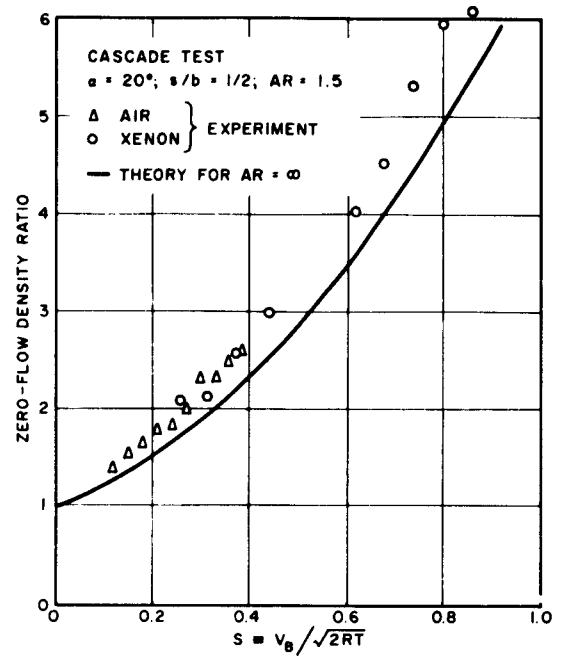


FIG. 33b

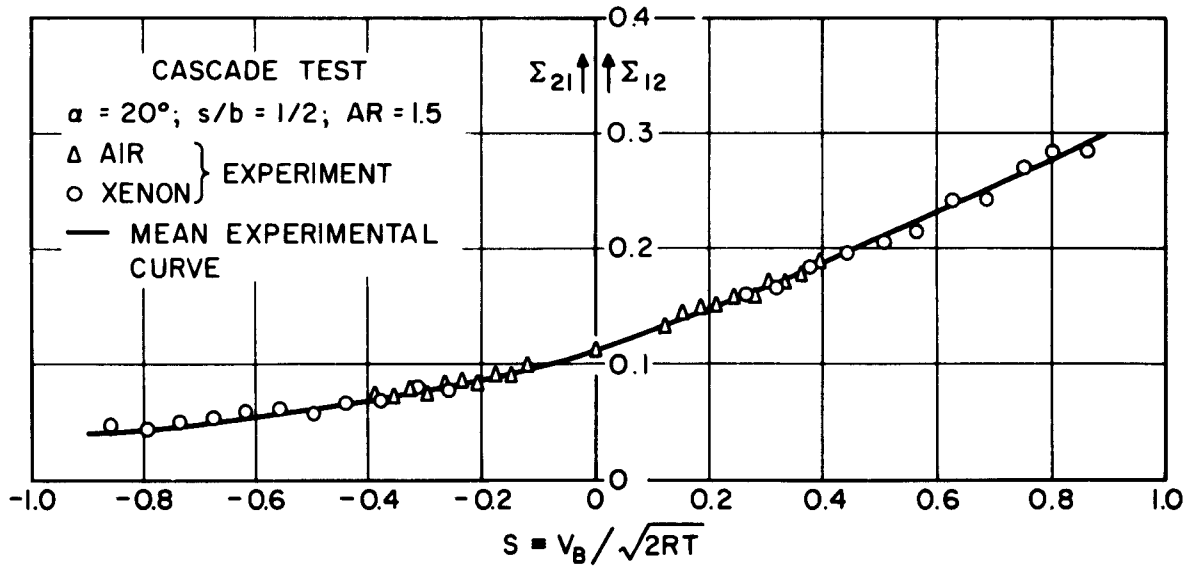


FIG. 33c

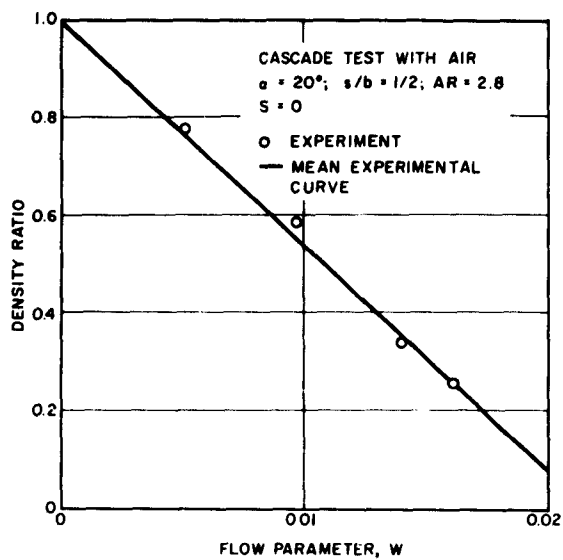


FIG. 34a

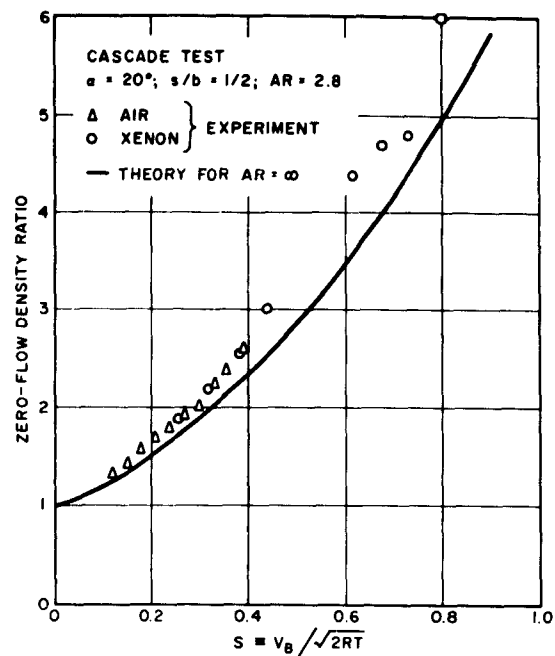


FIG. 34b

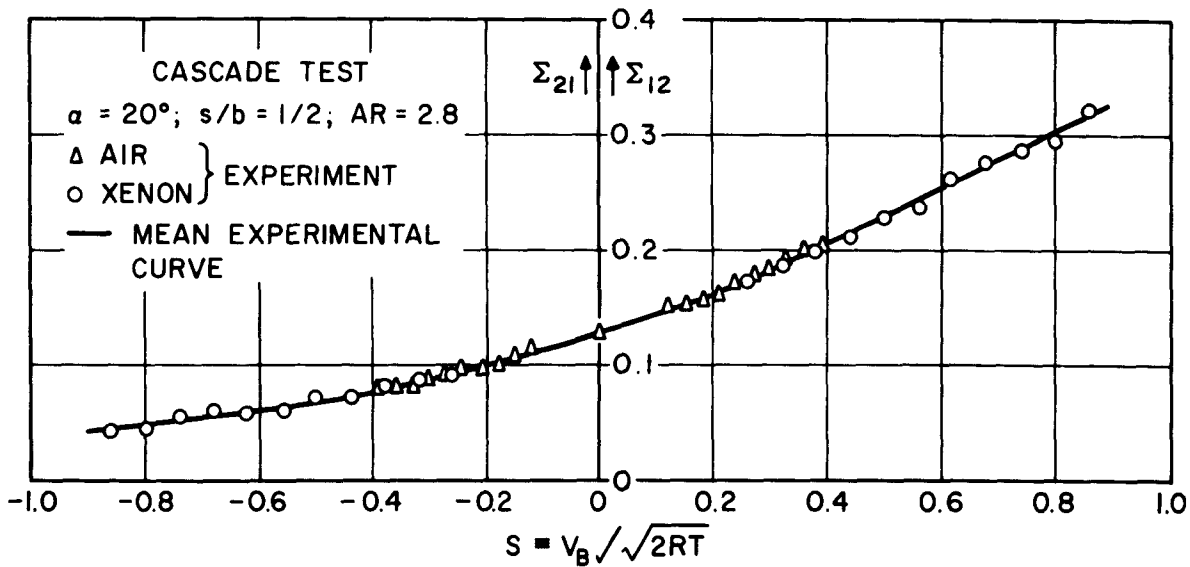


FIG. 34c

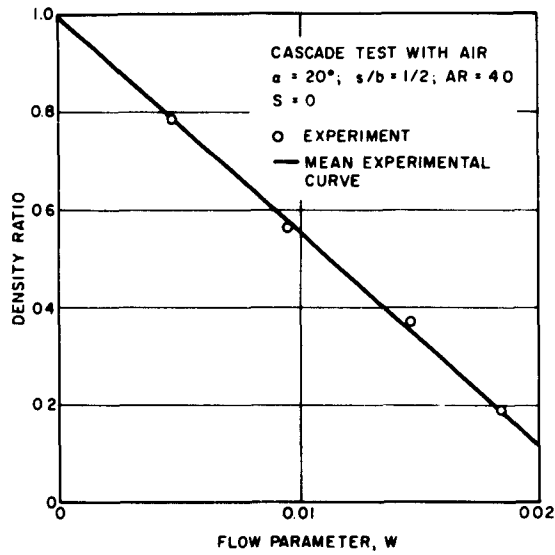


FIG. 35a

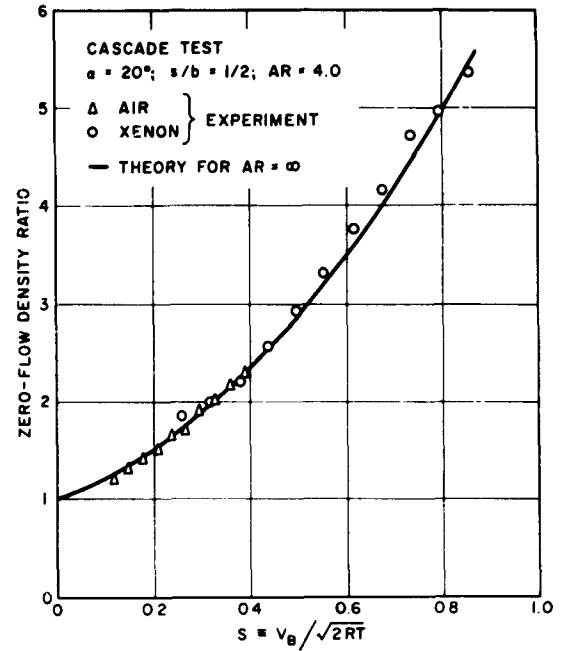


FIG. 35b

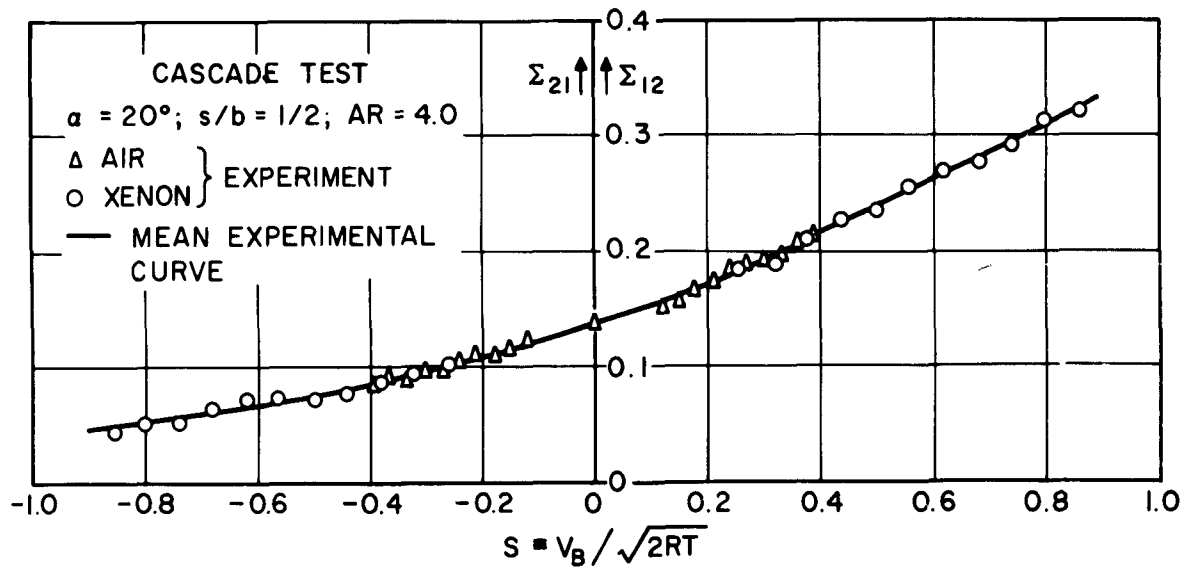


FIG. 35c

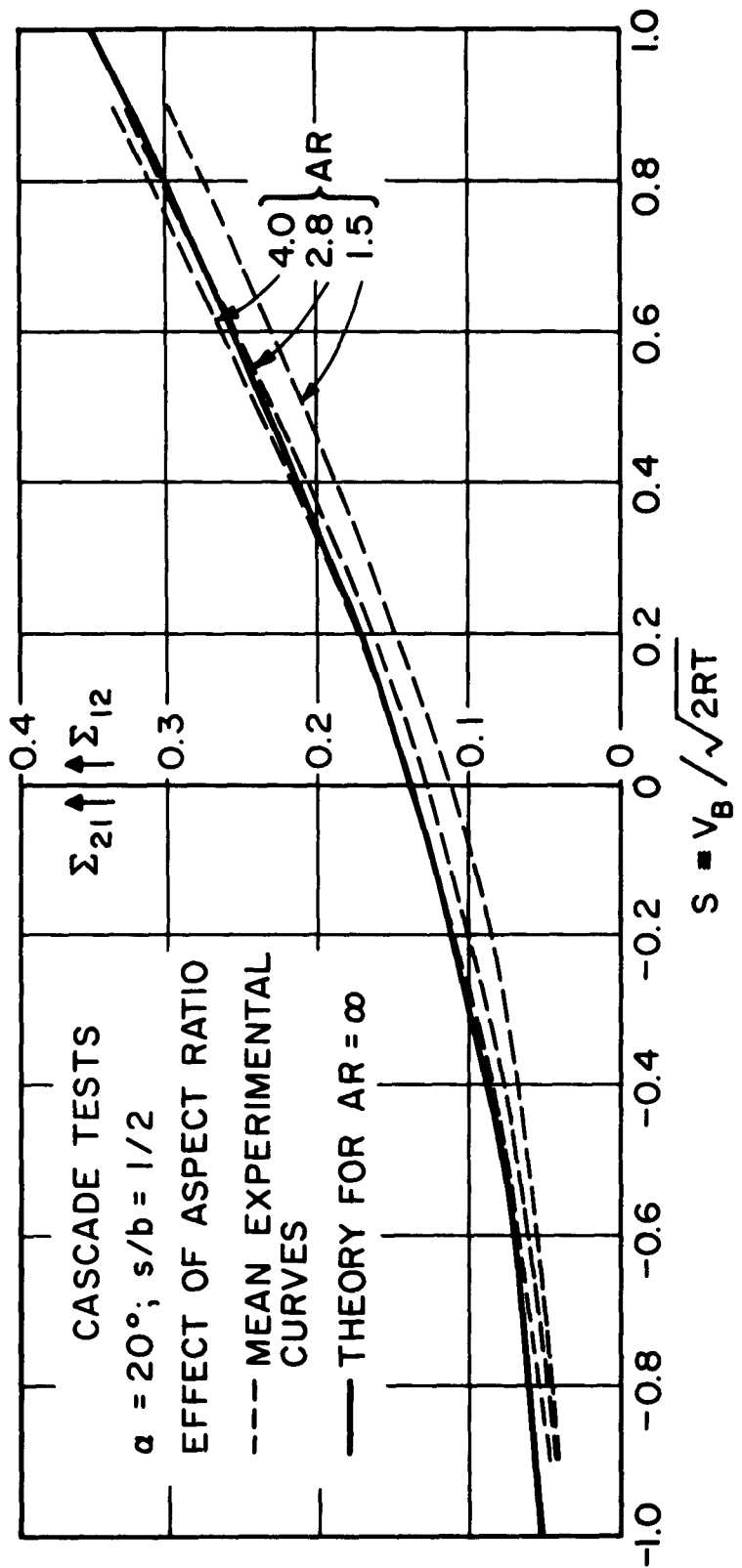


FIG. 36

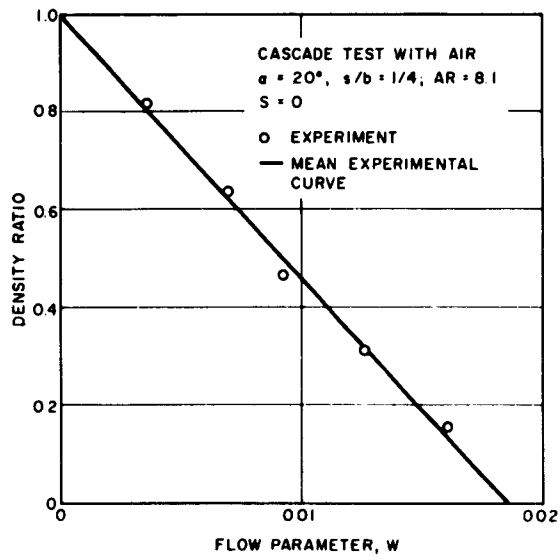


FIG 37a

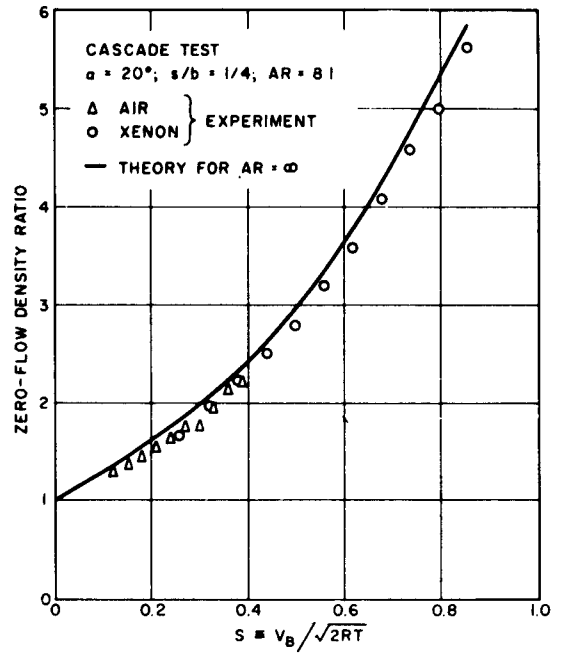


FIG 37b

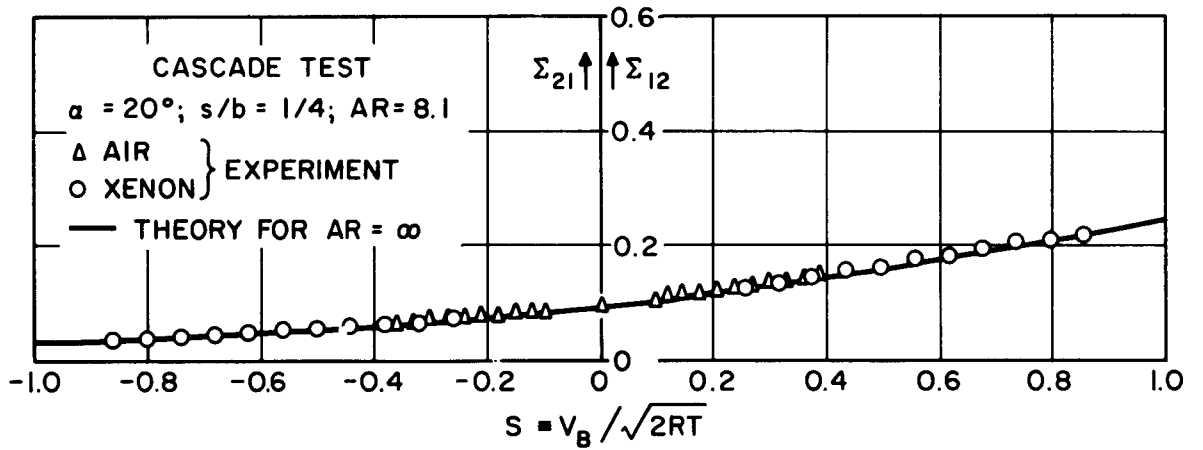


FIG. 37c

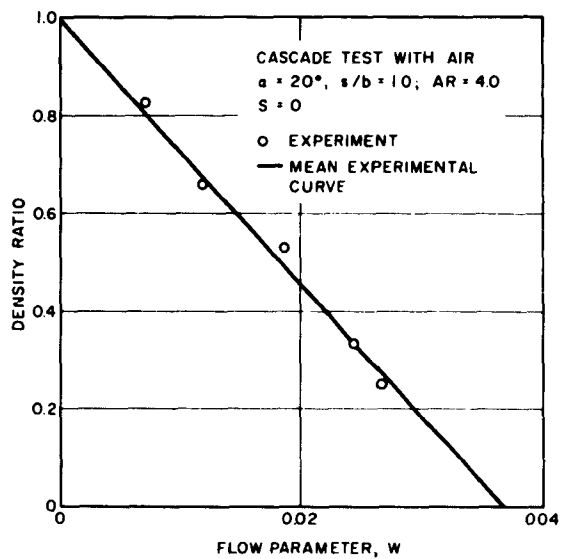


FIG. 38a

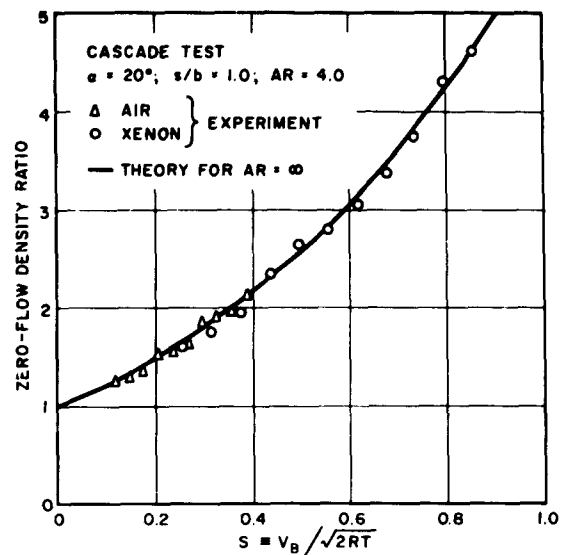


FIG. 38b

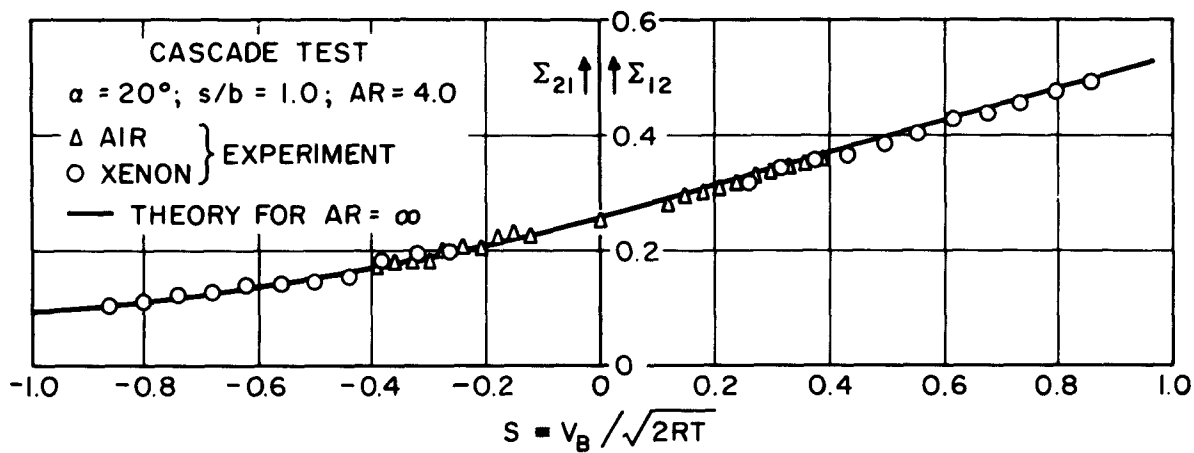


FIG. 38c

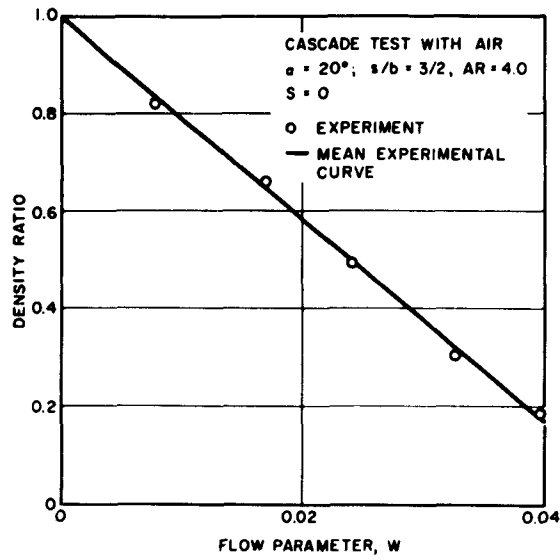


FIG. 39a

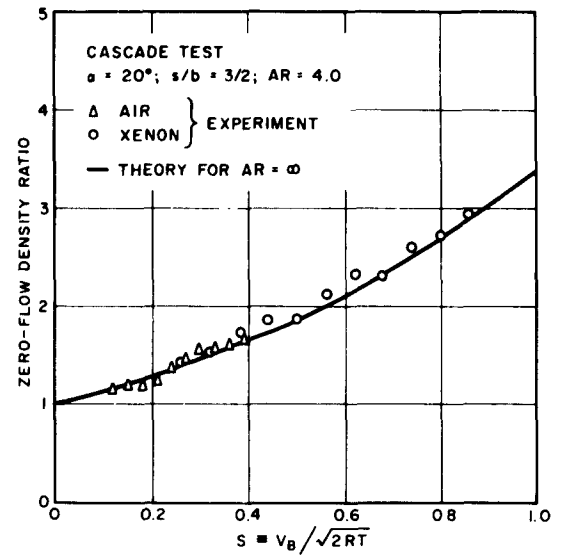


FIG. 39b

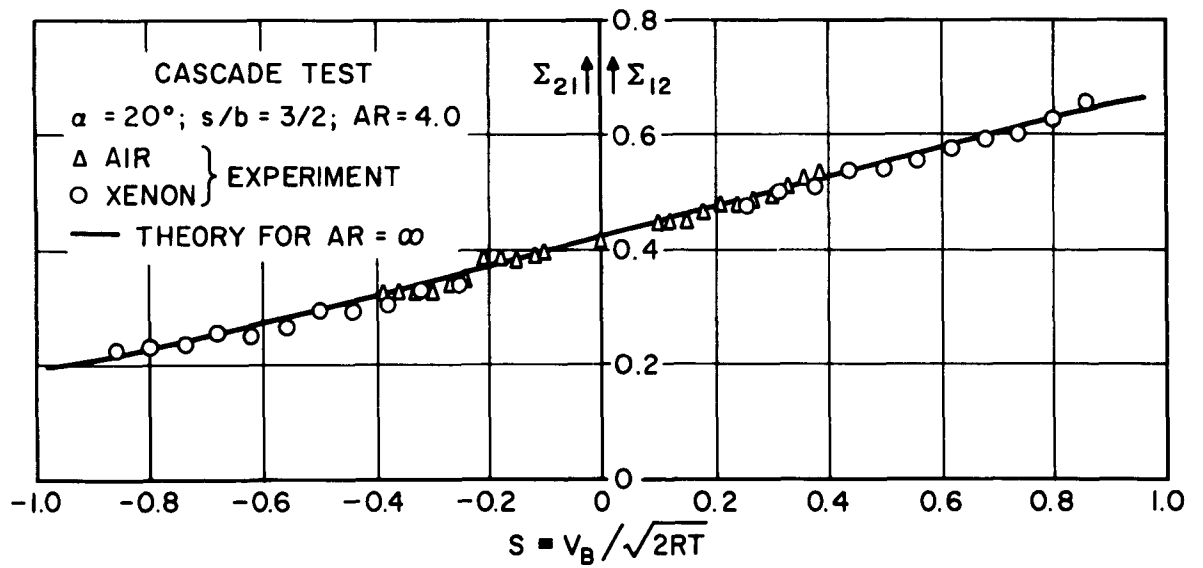


FIG. 39c

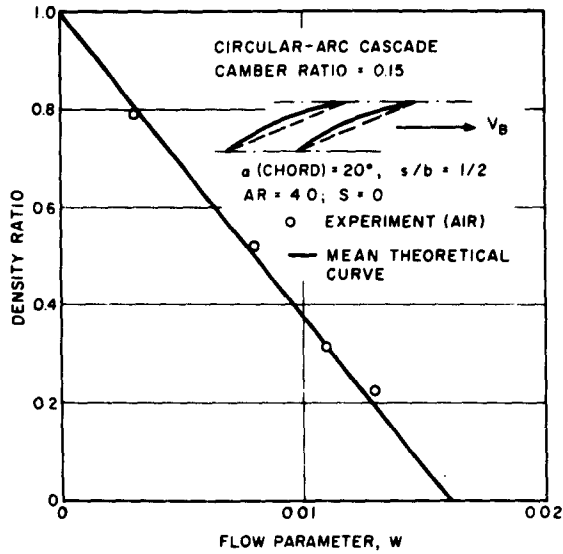


FIG. 40a

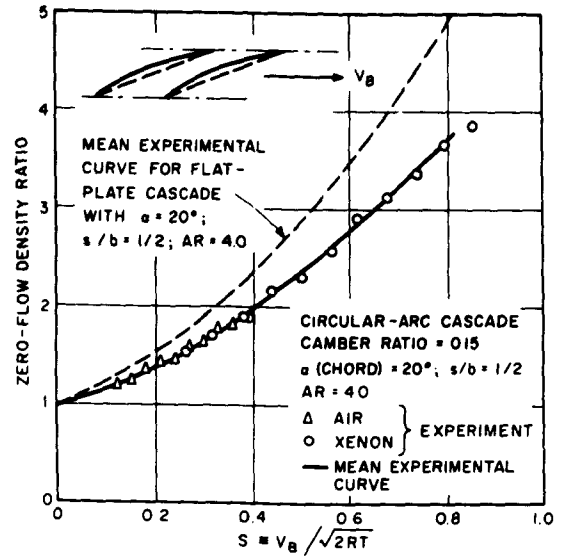


FIG. 40b

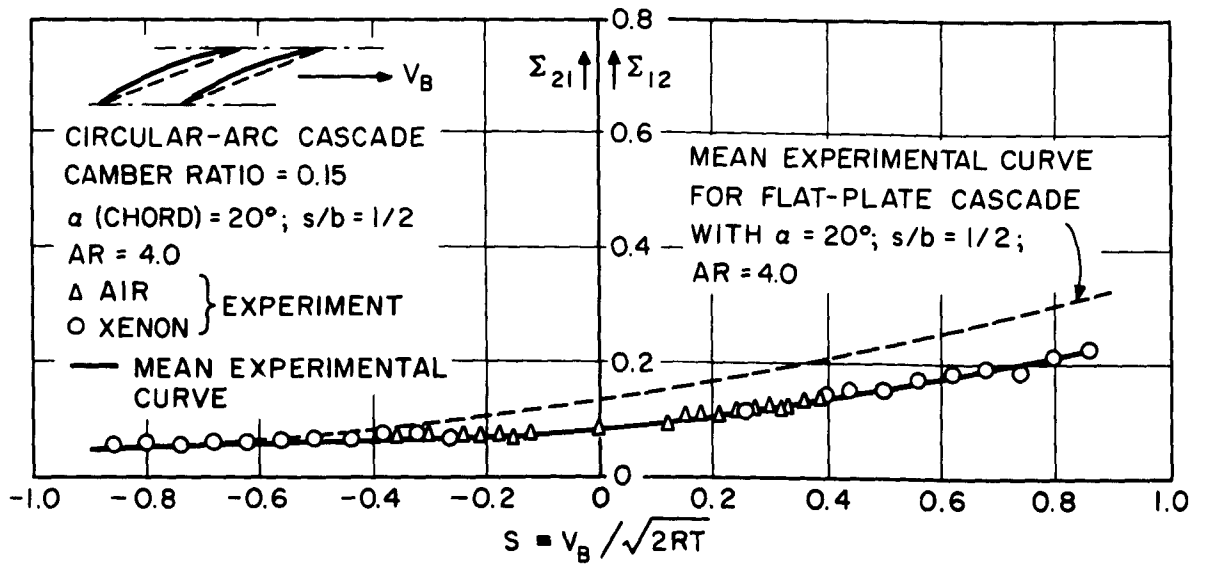


FIG. 40c

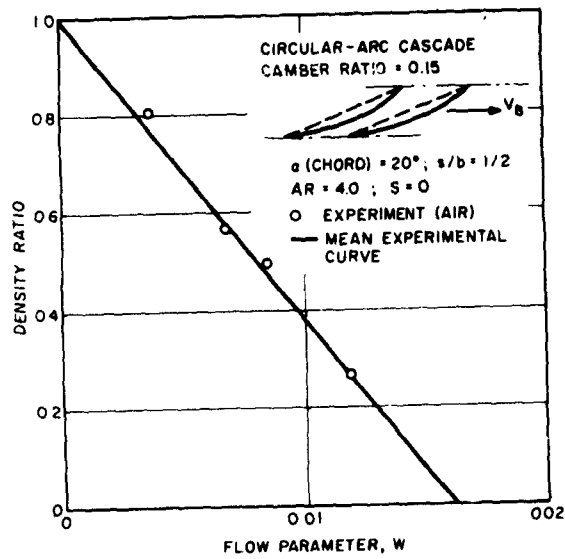


FIG 41a

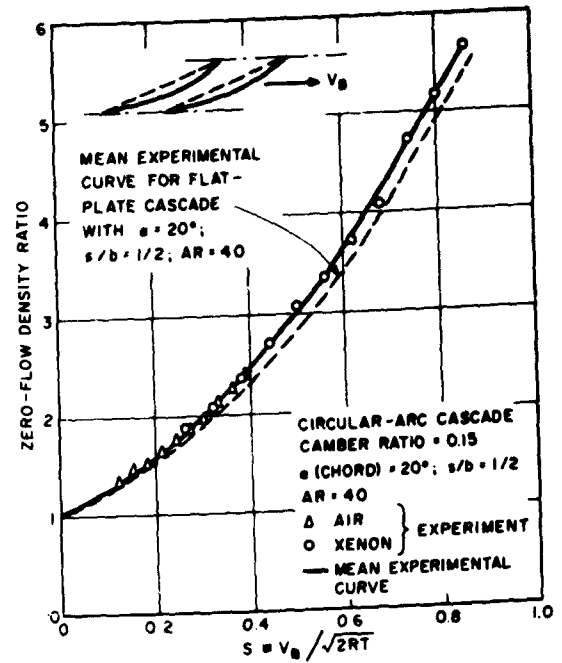


FIG. 41b

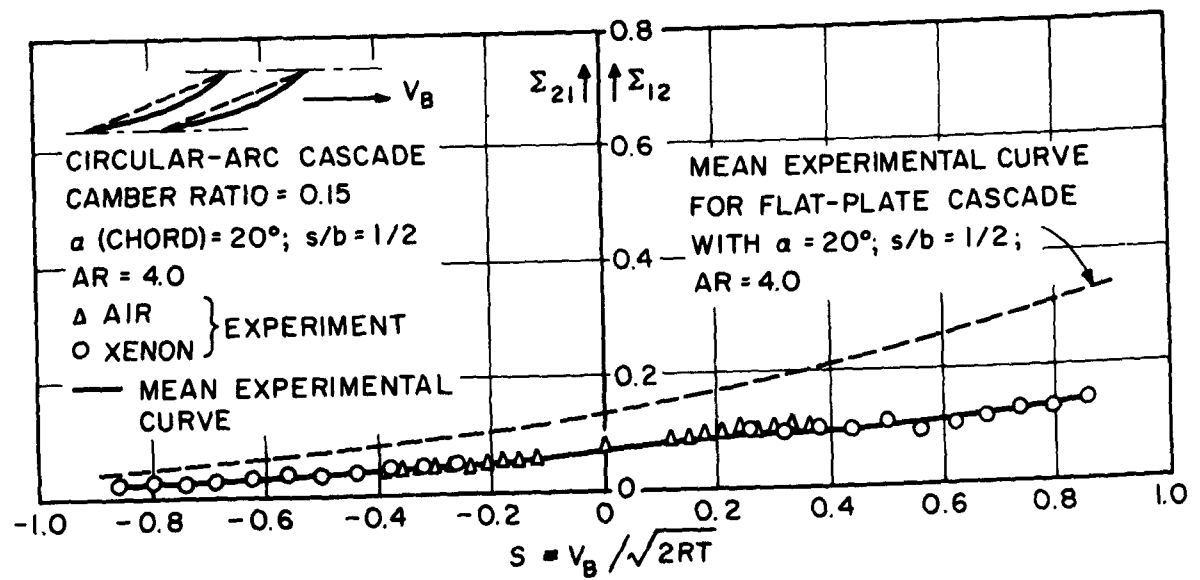


FIG. 41c